Fakultät für Physik und Astronomie

Ruprecht-Karls-Universität Heidelberg

Diplomarbeit

im Studiengang Physik

vorgelegt von

Sebastian Bock

aus **Neumünster**

September 2010

Higgs Physics at the LHC

Die Diplomarbeit wurde von Sebastian Bock
ausgeführt am
Institut für Theoretische Physik
unter der Betreuung von
Herrn Prof. Dr. Tilman Plehn

Higgs Physik am LHC

Die meisten Physiker erwarten, dass ein Higgs-Boson am LHC entdeckt wird. Zuvor muss das Higgs-Boson jedoch produziert werden. Aus diesem Anlass wird im ersten Teil der Arbeit der Wirkungsquerschnitt für den Gluon-Fusionsprozess ausgerechnet. Für diesen Prozess mit anschließendem Zerfall nach bottom-Quarks wurde eine Monte-Carlo Simulation geschrieben, die den totalen und die differentiellen Wirkungsquerschnitte für verschiedene physikalische Observablen in führender Ordnung bestimmt. Denkbar ist auch eine andere Realisierung des Higgs-Bosons als im minimalen Standard Modell. Diese Physik jenseits des Standard Modells kann Auswirkungen auf die Higgskopplungen haben. Deshalb wird im zweiten Teil der Arbeit die Modifikation der Kopplungen, hervorgerufen durch Wechselwirkungen mit einem versteckten Sektor und einem speziellen zusammengesetzten Higgsmodell, die am LHC zugänglich sind, untersucht. Beide Szenarien wirken sich ähnlich auf die Kopplungen aus, in dem sie universelle und teilweise universelle Modifikationen verursachen. Zusätzliche unsichtbare Zerfälle durch den Zerfall in den versteckten Sektor werden ebenfalls berücksichtigt. Experimentelle Grenzen an diese möglichen Modifikationen werden durch die Übereinstimmung eines beobachteten Higgs-Bosons mit dem Standard Modell bestimmt.

Higgs physics at the LHC

Most physicists expect to discover the Higgs boson at the LHC. But first the Higgs boson has to be produced. For this reason, we calculate the gluon-fusion Higgs production cross section in the first part. A Monte Carlo simulation for this process with subsequent decay to bottom quarks at leading order was written to obtain the total and differential cross sections with respect to physical observables. There can be other Higgs boson implementation as the minimal Standard Model. This physics beyond the Standard Model can affect the Higgs couplings. Thus, in the second part of this thesis, we study modifications through interactions with a hidden sector and in specific composite Higgs models accessible at the LHC. Both scenarios give rise to congruent patterns of universal, or partially universal, shifts. In addition, Higgs decays to the hidden sector may lead to invisible decay modes which we also exploit. Experimental bounds on such potential modifications will measure the concordance of an observed Higgs boson with the Standard Model.

Contents

List of Figures

1. Introduction

It is due to the ambition of mankind in the last centuries that we are able to think about the most elementary constituents of the universe and their dynamics. Approaching questions of such fundamental relevance is remarkable and fascinating at the same time. The laws of nature how they are realized in our universe make evolution possible to develop sufficiently intelligent life forms. This is the enchantment why people feel the necessity to reveal all laws of nature. Today, we can explore questions that were once originated from a philosophical point of view on profound footing of natural sciences.

Up to now, has been developed a profound theory that can explain every experiment in high energy physics. The Standard Model (SM) of elementary particles contains three of the four fundamental interactions the quantum electrodynamics (QED), weak interaction and quantum chromodynamics (QCD) with the corresponding gauge bosons photon γ, weak gauge bosons $W^{\pm}, Z^0$ and the gluons g and the matter particles which are six colour charged quarks and leptons of the same amount. The latter twelve particles are fermions and can be classified in three generations. In the Standard Model, symmetry and symmetry breaking play a crucial role.

From the claim that the Lagrangian is gauge invariant under local gauge transformations the fundamental interactions arise from gauge theories. Mathematically, these symmetries can be described by group theory with the Standard Model gauge group $SU(3)_C \times SU(2)_L \times U(1)_Y$. The Standard Model gauge group splits to QCD $SU(3)_C$ and the unification of the symmetries of weak interaction and electromagnetism $SU(2)_L \times U(1)_Y$, based on the work from Sheldon Glashow [6], Abdus Salam [7] and Steven Weinberg [5]. Local gauge transformations are only preserved if the gauge fields are massless. This leads to a problem because it is experimentally proven that the weak gauge bosons has a huge mass. For this reason, the electroweak symmetry must be broken.

Already in 1964, Peter Higgs [1], [2], Francois Englert, Robert Brout [3] and Thomas W. B. Kibble [4] found a solution for the symmetry breaking. By introducing a complex scalar field, which is an $SU(2)$ doublet called Higgs field that is charged under $U(1)_Y$ with an appropriate potential such that it acquires a vacuum expectation value, breaks the $SU(2)_L \times U(1)_Y$ electroweak symmetry to the $U(1)_Q$ gauge group of the electromagnetism. Three of the four degrees of freedom from the complex doublet are Goldstone bosons which are eaten by the three weak gauge bosons. Due to this, they give them a longitudinal polarization mode and their masses. The last degree of freedom is a physical observable

particle: the Higgs boson. Also the fermions get their masses from the Higgs field by Yukawa couplings.

The Higgs sector in the Standard Model is highly hypothetical. No Higgs boson has been observed yet. From LEP at CERN where electron positron collisions were observed, we know that the Higgs boson must be heavier than 114 GeV [8]. There are also theoretical constraints on the mass. From the renormalization group equation for the quartic Higgs coupling [9], which describes the energy dependence of that coupling because of divergences in higher order corrections, follows the stability and triviality bound. The running coupling has a singularity at a certain energy scale. Up to this scale, we can rely on the perturbative theory. This point depends on the Higgs mass and is called triviality bound [10]. The stability bound [12] is given by the condition that the quartic Higgs coupling has to be bigger than zero because only then the Higgs potential is bounded from below. At the Planck scale (10^{19} GeV) these two bounds predict a Higgs mass of around 180 GeV to 190 GeV [11].

At the moment, nobody knows how the electroweak symmetry is broken at the TeV scale. This was one of the major aspects for constructing the LHC. Over the years, scientists developed alternative or extended models to explain electroweak symmetry breaking. Having only one Higgs doublet is preferred to keep the theory as easy as possible. Alternatively, we can think about introducing another doublet. There are three different types of two Higgs doublet models. In the first one, only one Higgs doublet couples to both up- and down-type fermions and the other does not couple to any fermion [13]. In the second type of model, one of the two Higgs doublet couples to up- and the other to down-type fermions [14]. And the third type of model allows all kinds of possible couplings [15]. In all of these models, more than one Higgs boson appears.

In the Higgs sector occurs a problem which is referred to as the hierarchy problem. From higher order perturbative corrections, divergences appear in the Higgs mass or Higgs potential parameter, e.g. the one loop contribution from the top-Quark is quadratically divergent. We can introduce a cut-off to keep it finite. But this means that the theory is limited to a certain energy. For this reason, the Standard Model is expected to be only a low energy limit of a more fundamental theory. Also the huge amount of free parameters in the Standard Model is another hint. One solution for this problem is Supersymmetry [24] which transforms a boson to a fermion and vice versa. It means that every boson (fermion) has a corresponding supersymmetric fermion (boson). If this symmetry is exact then the quadratic divergences from the loop corrections to the tree level parameters cancel exactly because fermion loops have an additional minus sign in comparison to boson loops. But supersymmetry is not an exact symmetry because otherwise we would have observed supersymmetric partners of the Standard Model particles predicted from Supersymmetry.

Also models with extra dimensions was once motivated by String Theory became popular in the last decade. There are models with large extradimension as in the Arkami-Hamed, Dimopoulos and Dvali (ADD) model [21] or with warped extra dimensions as in

the Randall-Sundrum model [22]. Basing on these approaches, models with or without a Higgs boson are invented. One class of model is the minimal composite Higgs model (MCHM) [124–126] where the Higgs boson appears as a pseudo-Goldstone boson from new strong dynamics. This model takes advantage of the holographic principle that is based on the AdS/CFT correspondence [23], where strongly-coupled theories in four dimensions are identified with weakly-coupled theories in five dimensions. The minimal composite Higgs model predicts a shift in the Higgs couplings of the minimal Standard Model.

In general, mass is a strange thing. Everybody has a good feeling about what mass means but nobody can explain where it comes from. We know since centuries that masses attract each other by gravity. But only from the beginning of the 20th century on, people got new fundamental insights into mass, energy and space-time. In 1905, Albert Einstein formulated the special theory of relativity [16] that yields a relation between mass and energy. It means that energy and mass can be transformed into each other. This relation is proven over and over again in particle colliders where it is used to produce heavier particles.

Ten years later general relativity [17] was found and it is still the best theory of gravity. It is a classical field theory. Today, no quantum field theory of gravity is known so that it cannot be a part of the Standard Model. Scientists are looking for hints like a graviton that would be the mediator of the gravitational force. But also the graviton has not yet been observed. Since gravity is very weak, it does not play a role in nowadays collider physics.

From astronomical observations in the last two decades, we know that only 5 % of our universe is made up from known particles [19]. The rest splits into 23 % dark matter and 72 % dark energy. In the observation of galactic rotations, there occurred a discrepancy between the theoretical prediction and the measurement. One solution is that there is more matter than we can see because it interacts only very weak that is called dark matter. Another explanation is that our theory of gravity is not valid at all distances [18]. The first solution is much preferred. We also observe an accelerating universe [20] that demands something like negative pressure that is called dark energy. Probably, the LHC will teach us more about these topics.

As we have seen, there are unexplained things in nature. Some of these things will hopefully be solved at the LHC, but others are still beyond the possibilities of the LHC. So there is still a lot of work that has to be done in the next decades. But there is a good chance to reveal the electroweak symmetry breaking mechanism in the near future. Such knowledge would lead to a limited class of models.

2. LHC physics

2.1. Gluon-fusion process

At the LHC, there are four Higgs-boson production processes, see Fig. (2.1). On the experimental side, the gluon-fusion (GF) process has the biggest cross section. And on the theoretical side, it is the most challenging process to compute because of the top-loop. For that reasons, it is worth it to study this process in more detail.

In the SM, there is no direct coupling between gluons and Higgs-boson. That is why another particle is needed to connect them with each other. The top-quark is a good choice for this particle because it has the biggest coupling constant to the Higgs-boson due to its huge mass that is proportional to the coupling. The top-loop coupling corresponds to an effective Lagrangian [61] that is given by

$$\mathscr{L} \propto H G_{\mu\nu} G^{\mu\nu}, \tag{2.1}$$

where H is the Higgs field and $G_{\mu\nu}$ is the QCD field strength tensor.

2.1.1. Higgs production cross section

The first step in calculating a cross section is putting together all the Feynman rules [50] that are needed for the diagram and writing down the matrix element. For the gluon-fusion process, three fermion propagators, two gluon couplings to fermions, one loop integral, one Yukawa coupling and a minus sign for the fermion loop are needed. In the following, g_S denotes the strong gauge coupling, m the top-quark mass, p_i the four-momentum vectors of the incoming gluons, ϵ_i the gluon polarization vectors, γ the Dirac matrix, T the $SU(3)$ group generators and G_F the Fermi constant. The matrix element for the GF process can then be written as

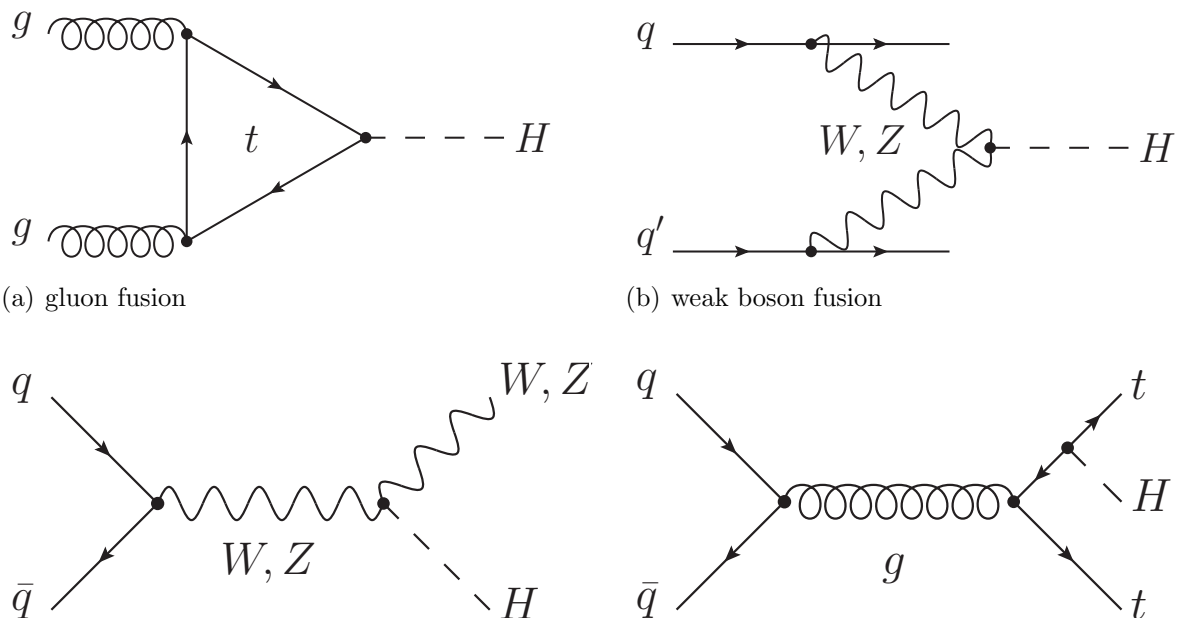

(a) gluon fusion

(b) weak boson fusion

(c) Higgs strahlung

(d) heavy quarks associated Higgs production

Figure 2.1.: Shows the four major partonic Higgs production processes at the LHC.

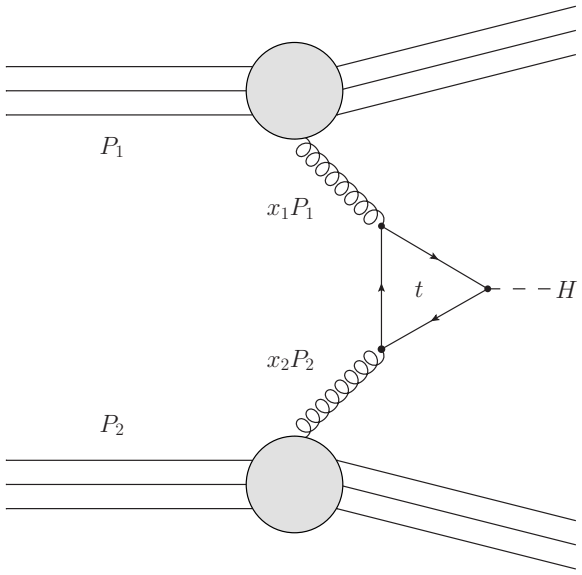

Figure 2.2.: Depicts the hadronic gluon-fusion process at the LHC. P_1 and P_2 denote the two incoming protons.

$$\begin{aligned}\mathcal{M} =& -\int \frac{d^4q}{(2\pi)^4}\,\mathrm{Tr}\left[\epsilon_1^\mu(-ig_S\gamma_\mu T^a_{jk})\frac{i(\not{q}+\not{p}_1+m)}{(q+p_1)^2-m^2}(-ig_S\gamma_\nu T^b_{kj})\epsilon_2^\nu\frac{i(\not{q}+\not{p}_1+\not{p}_2+m)}{(q+p_1+p_2)^2-m^2}\right.\\ &\left.(-im(\sqrt{2}G_F)^{\frac{1}{2}})\frac{i(\not{q}+m)}{q^2-m^2}\right]\\ =&\frac{1}{4\pi}(\sqrt{2}\,G_F)^{\frac{1}{2}}\,\alpha_S\,m\;\mathrm{Tr}(T^aT^b)\,\epsilon_1^\mu\,\epsilon_2^\nu\,F\,P_{T\mu\nu}\,.\end{aligned} \tag{2.2}$$

Because of the fermion loop, the trace is applied only to the occurring Dirac matrices. The relation $\alpha_S = \frac{g_S^2}{4\pi}$ for the strong coupling constant is used. F (explicitly defined in Eq. (2.5)) is the form factor of the effective gluon-gluon-Higgs coupling and $P_{T\mu\nu} = \eta^{\mu\nu} - \frac{p_1^\mu p_2^\nu}{p_1\cdot p_2}$ is a transverse projector. Due to the fact that gluons are massless, they only have transverse components. For this reason, one can introduce the transverse projector without losing any information. The calculation of the Dirac trace can be done by hand or using a tool like FORM [25, 26] that can do it. The result is

$$\begin{aligned}T^{\mu\nu} =& \,\mathrm{Tr}\left[\gamma^\mu\left(\not{q}+\not{p}_1+\not{p}_2+m\right)\left(\not{q}+m\right)\gamma^\nu\left(\not{q}+\not{p}_1+m\right)\right]\\ =&4m\,(4q^\mu q^\nu + 2q^\mu p_1^\nu + 2q^\nu p_2^\mu + 4q^\nu p_1^\mu\\ &+ p_2^\mu p_1^\nu + p_2^\nu p_1^\mu + 2p_1^\mu p_1^\nu + \eta^{\mu\nu}m^2\\ &-\eta^{\mu\nu}q\cdot q - 2\eta^{\mu\nu}q\cdot p_1 - \eta^{\mu\nu}p_1\cdot p_2 - \eta^{\mu\nu}p_1\cdot p_1)\end{aligned} \tag{2.3}$$

and applying the transverse projector to it yields

$$P_{T\mu\nu}T^{\mu\nu} = 4m\left(3m^2 - m_H^2 - \frac{8}{m_H^2}p_{1\mu}p_{2\nu}q^\mu q^\nu - 2p_{1\mu}q^\mu + \eta_{\mu\nu}q^\mu q^\nu\right). \tag{2.4}$$

Because of the loop momenta in this expression tensor integrals $C^{\mu\nu}$ and C^μ in F appear. In App. A I explain how to reduce them to scalar integrals. The method is called Passarino Veltman reduction. For F, one finds [28]

$$\begin{aligned}F =& \frac{1}{2}P_T^{\mu\nu}\int\frac{d^4q}{i\pi^2}\frac{\mathrm{Tr}[(\not{q}+m)\gamma_\mu(\not{q}+\not{p}_1+m)\gamma_\nu(\not{q}+\not{p}_1+\not{p}_2+m)]}{(q^2-m^2)((q+p_1)^2-m^2)((q+p_1+p_2)^2-m^2)}\\ =&\,2m + m(4m^2-m_H^2)C_0(p_1,p_2,m)\,.\end{aligned} \tag{2.5}$$

Here, C_0 denotes the 3-point scalar function, which is calculated in App. B in full detail. The result is

$$C_0(p_1,p_2,m) = \begin{cases} -\frac{2}{m_H^2}\arcsin^2\left(\sqrt{\frac{1}{\rho}}\right), & \rho > 1 \\ \frac{1}{2m_H^2}\left(\log\left(\frac{1+\sqrt{1-\rho}}{1-\sqrt{1-\rho}}\right) - i\pi\right)^2, & \rho < 1 \end{cases}, \quad \rho = \frac{4m^2}{m_H^2}\,. \tag{2.6}$$

Now the matrix element is completely determined. The last step is squaring the matrix element and averaging over all possible initial states, that means the polarizations and the adjoint representation of the gluons, because the beams are not polarized. The averaged squared matrix element is

$$\begin{aligned} \overline{|\mathcal{M}|^2} &= \frac{1}{2\cdot 2\cdot 8\cdot 8}\sum_{\text{pols}}\sum_{a,b=1}^{8}\mathcal{M}^2 \\ &= \frac{G_F\,\alpha_S^2\,m^2}{128\sqrt{2}\pi^2}F^2. \end{aligned} \tag{2.7}$$

What we calculated so far is the matrix element of the partonic process (Fig. 2.1). But at the LHC, two protons collide head-to-head. Therefore, we are interested in the hadronic cross section (Fig. 2.2). In hard parton processes, the hadronic cross section is given by

$$\sigma_{tot} = \int dx_1 \int dx_2\, f(x_1)\, f(x_2)\sigma_{tot}^{part}(x_1,x_2)\,. \tag{2.8}$$

where x_1 and x_2 are the longitudinal momentum fractions of each proton that is carried by a parton and f is the parton distribution function. A hadron is a pretty sophisticated object. It doesn't only consist of the valence quarks but also of sea quarks. Due to the uncertainty relation, quarks, antiquarks and gluons can be created if they annihilate in a certain period of time. These dynamical objects are the so-called sea. They also carry a non-negligible amount of the hadron momentum. Thus, f gives the probability for finding a certain parton at longitudinal momentum fraction x. We are interested in gluons.

Therefore, using the longitudinal momentum fractions x_1 and x_2 the center of mass energy of the partonic process s can be expressed by the hadronic com energy S through

$$s = p_1 + p_2 = x_1P_1 + x_2P_2 = \left(\begin{pmatrix} x_1E \\ 0 \\ 0 \\ x_1E \end{pmatrix} + \begin{pmatrix} x_2E \\ 0 \\ 0 \\ -x_2E \end{pmatrix}\right)^2 = 4x_1x_2E = x_1x_2S\,, \tag{2.9}$$

where P_1 and P_2 are the incoming proton momenta with energy E. If the LHC operates at full power then the energy of a proton is $E = 7\,\text{TeV}$ which is much bigger than its mass. For this reason the proton's mass can be neglected.

In the following calculation, it is easier to change the variables from x_1, x_2 to τ, y given by the relations

$$\tau = x_1 x_2,\ y = \frac{1}{2}\log\left(\frac{x_1}{x_2}\right);\ x_1 = \sqrt{\tau}\exp(y),\ x_2 = \sqrt{\tau}\exp(-y);\ dx_1 dx_2 = d\tau dy\,. \quad (2.10)$$

The cross section is Lorentz invariant under boosts along the beam axis. For this reason, the calculation can be done in the center of mass frame. That means, the Higgs boson is created at rest

$$\begin{aligned}
\sigma_{tot}^{gg\to H} =& \int dx_1 \int dx_2\, f(x_1)\, f(x_2) \int \frac{\overline{|\mathcal{M}|^2}}{2s}(2\pi)^4\,\delta^4(k_1+k_2-p)\frac{d^3p}{(2\pi)^3 2p_0} \\
=& \int d\tau \int dy\,\tau\, f(\sqrt{\tau}\,\exp(y))\, f(\sqrt{\tau}\,\exp(-y))\,\frac{\pi\overline{|\mathcal{M}|^2}}{\tau^2 S^2}\delta(\tau-\tau_0) \\
=& \frac{G_F\alpha_S^2}{128\sqrt{2}\pi}\,\rho^2\left(1+(1-\rho)\arcsin^2\left(\sqrt{\frac{1}{\rho}}\right)\right)^2 \\
& \int dy\, f(\sqrt{\tau_0}\exp(y))\, f(\sqrt{\tau_0}\exp(-y))\,.
\end{aligned} \quad (2.11)$$

In the last step, I plugged in the light Higgs solution. The light Higgs solution is also used in the following because it is in favor.

2.1.2. Higgs decay cross section to $b\bar{b}$

The Higgs boson is a very short lived particle thus it will never be observed directly. The detectors can only measure the decay remnants. Up to a Higgs mass of 160 GeV the decay is dominated by the bottom quarks. So for this reason let's have a look at a gluon fusion produced Higgs boson with subsequent decay to bottom quarks.

m_H [GeV]	BR [1]	Γ [GeV] 31-35
120	0.67	$3.60 \cdot 10^{-3}$
240	$0.13 \cdot 10^{-2}$	3.40
480	$0.13 \cdot 10^{-3}$	59.06

Table 2.1.: The branching ratio BR and decay width Γ of the Higgs boson is shown for three different Higgs masses m_H. The values are from HDECAY [119].

Narrow width approximation

A light Higgs boson has a small decay width such that we can approximately treat it like a stable on mass shell particle. In this case, the total cross section separates into the production cross section times the branching ratio

$$\begin{aligned}\sigma_{tot} &= \sigma_{tot}^{gg\to H}\,\mathrm{BR}(H\to b\bar{b}) \\ &= \frac{G_F\alpha_S^2}{128\sqrt{2}\pi}\,\rho^2\left(1+(1-\rho)\arcsin^2\left(\sqrt{\frac{1}{\rho}}\right)\right)^2 \\ &\quad \int dy\, f(\sqrt{\tau_0}\exp(y))\, f(\sqrt{\tau_0}\exp(-y))\,\mathrm{BR}(H\to b\bar{b})\,.\end{aligned} \tag{2.12}$$

We only have to multiply the production cross section with the branching ratio of the decay. The branching ratio is the fraction of the decay width of the decay channel and the total decay width. It gives the probability that a Higgs boson decays to bottom quarks. From Table 2.1 follows that the decay has a probability of 67.3 % when the Higgs boson has a mass of 120 GeV.

Breit-Wigner propagator

In the narrow width approximation (NWA), the Higgs boson is treated like a real particle that is always on mass-shell. But it is a highly unstable particle where it is produced as a virtual particle that is smeared out around the Higgs mass (off mass-shell). For this reason, to get a more realistic result, the Dirac delta function has to be replaced by a function that approximates it such that the mass is distributed around a mean value. One possible approximation is a Breit-Wigner (BW) function [29]

$$\lim_{\Gamma\to 0}\frac{1}{(s-m_H^2)^2+m_H^2\Gamma^2} = \frac{\pi}{m_H\Gamma S}\delta(\tau-\tau_0) \quad\Rightarrow\quad \delta(\tau-\tau_0)\approx\frac{Sm_H\Gamma/\pi}{(s-m_H^2)^2+m_H^2\Gamma^2} \tag{2.13}$$

But why did we use a Breit Wigner and not, e.g., a gaussian that can approximate it, too? The propagator of a particle has, at leading order, a singularity at the mass. But if we consider all one loop vacuum polarizations, that means summing over all one particle irreducible M^2, the propagator looks like

$$\frac{\mathrm{i}}{p^2 - m_H^2} \to \frac{\mathrm{i}}{p^2 - m_{H,0}^2 - M^2(p^2)}\,, \tag{2.14}$$

where $m_{H,0}$ is the bare mass term in the non-renormalized Lagrangian. The physical mass is the defined by

$$m_H^2 - m_{H,0}^2 - \mathrm{Re}(M^2(m_H^2)) = 0\,. \tag{2.15}$$

We can expand this equation around $p^2 \approx m_H^2$, which gives

$$\begin{aligned} p^2 - m_{H,0}^2 - M^2(p^2) \approx & p^2 - m_{H,0}^2 - \mathrm{Re}(M^2(m_H^2)) - (p^2 - m_H^2)\, \frac{d}{dp^2}\,\mathrm{Re}(M^2(p^2))\Big|_{p^2=m_H} \\ & + \mathrm{i}\,\mathrm{Im}(M^2(m_H^2)) \\ = & \left(1 + \frac{d}{dp^2}\,\mathrm{Re}(M^2(p^2))\Big|_{p^2=m_H}\right)\left(p^2 - m_H^2\right) + \mathrm{i}\,\mathrm{Im}(M^2(m_H^2)) \\ = & Z^{-1}\left(p^2 - m_H^2\right) + \mathrm{i}\,\mathrm{Im}(M^2(m_H^2))\,. \end{aligned} \tag{2.16}$$

In the last step, we introduced the field renormalization factor Z, which is defined by $Z^{-1} = 1 + \frac{d}{dp^2}\,\mathrm{Re}(M^2(p^2))\Big|_{p^2=m_H}$. The imaginary part of the vaccum polarization can be linked to the total decay width according to the optical theorem

$$\mathrm{Im}(M^2(m_H^2)) = -Z^{-1} m_H \Gamma\,. \tag{2.17}$$

Now, the propagator of Eq. (2.14) is determined. The cross section is proportional to the modulus squared propagator which reads

$$\sigma \propto \left|\frac{1}{s - m_H^2 + i m_H \Gamma}\right|^2 = \frac{1}{\left(s - m_H^2\right)^2 + m_H^2 \Gamma^2}\,. \tag{2.18}$$

Replacing the Dirac delta function in Eq. (2.11) with the relation of Eq. (2.13), we get the more realistic result for the total cross section.

$$\begin{aligned}\sigma_{tot} =& \frac{G_F \alpha_S^2}{128\sqrt{2}\pi} \int d\tau \int dy\, \tau\, f(\sqrt{\tau}\exp(y))\, f(\sqrt{\tau}\exp(-y)) \\ & \rho^2 \left(1 + (1-\rho)\arcsin^2\left(\sqrt{\frac{1}{\rho}}\right)\right)^2 S \frac{m_H \Gamma/\pi}{(s-m_H^2)^2 + m_H^2\Gamma^2}\, \mathrm{BR}(H \to b\bar{b})\,.\end{aligned} \tag{2.19}$$

With this formula, we will see a resonance at m_H, that means the cross section is enhanced around that point.

2.1.3. Heavy top-quark limit

In the case when the top-quark mass is much bigger than the Higgs mass, the limit

$$\lim_{\rho\to\infty} \rho \left(1 + (1-\rho)\arcsin^2\left(\sqrt{\frac{1}{\rho}}\right)\right) = \frac{2}{3}\,, \tag{2.20}$$

can be performed with the Taylor expansion of the inverse sine function [53]

$$\arcsin^2\left(\sqrt{\frac{1}{\rho}}\right) = \left(\frac{1}{\rho^{\frac{1}{2}}} + \frac{1}{6\rho^{\frac{3}{2}}} + \mathcal{O}(\rho^{-\frac{5}{2}})\right)^2 = \frac{1}{\rho} + \frac{1}{3\rho^2} + \mathcal{O}(\rho^{-3})\,. \tag{2.21}$$

The top-quark is not a propagating particle any more and the form factor gets independent of the top-quark mass.

2.2. Monte Carlo program for gluon-fusion process

In physics and in particular in high energy physics computer programs and simulations are widely used. There is a class of algorithm which is called Monte Carlo because it is based on pseudo random numbers. According to this, physicists in the 40's who were working on the nuclear weapon project in Los Alamos gave the name to it. On a computer, random numbers are generated using some algorithm; therefore, they cannot really be random numbers. Over the last decades, people tried to improve these algorithms to make the random numbers more and more statistical independent to get them closer to random numbers.

In high energy physics, Monte Carlo methods are good tools to simulate experiments, detectors or to calculate integrals which are very difficult or even unfeasible to calculate analytically. For instance, SHERPA [30] and PYTHIA [31] are two event generators using Monte Carlo techniques.

2.2.1. Integrating functions and making histograms

Assume we want to integrate a function f that depends on two variables $x \in [a, b] = I_x$ and $y \in [c, d] = I_y$. We can calculate the integral with random numbers using the mean value theorem [53]. That means, we need to calculate the mean value of the function in the domain and multiply it with the area of the domain. Therefore, we generate two random numbers x_i and y_i in the appropriate interval and calculate the value of f at this point. This sampling must be done N times. Mathematically spoken,

$$A = \int_c^d \int_a^b f(x, y) dx dy \approx \frac{(c-d)(b-a)}{N} \sum_{i=1}^{N} f(x_i, y_i) \,. \tag{2.22}$$

The error of the integral is decreasing with increasing sampling size. Hence, we have to pay attention that the sampling size is sufficiently large. This method is plain Monte Carlo. It assumes that f is "gutartig". For other functions it is better to use an improved method, important sampling [51].

With the described method, we are able to calculate the total cross section. But we are also interested in histograms of differential cross sections, which I want to explain now. Assume we are interested in a histogram of the derivative of f with respective to y. For this, we need to divide the interval of y into n equidistant pieces:

$$I_y = \bigcup_{i=0}^{n-2} [c_i, d_i) \cup [c_{n-1}, d_{n-1}] \quad \text{with} \quad I_y^k \cap I_y^j = \emptyset, \quad k \neq j, \quad k, j \in \{0, \ldots, n-1\} \,. \tag{2.23}$$

The discrete histogram function h containing n bins with bin width $\frac{d-c}{n}$ is then defined by

$$h(k) = \frac{(c-d)(b-a)}{N} \sum_{i=1}^{n_k} f(x_i, y_i), \quad y_i \in I_y^k, \quad k \in \{0, \ldots, n-1\}, \quad \sum_{i=0}^{n-1} n_k = N \,. \tag{2.24}$$

Also y is discretized by a function Y

$$Y(k) = c + k\frac{d-c}{n}, \quad k \in \{0, \ldots, n-1\} \,. \tag{2.25}$$

The last step is to write all the pairs $(Y(k), h(k))$ into a file and plot them with a program, e.g., gnuplot.

2.2.2. Generating events

We are interested in physical quantities of the final state particles, e.g., the scattering angle, the energy. But in the calculation of the gluon-fusion process, we only calculated the production cross section and multiplied it with the branching ratio of the decay channel. In a two to two scattering process there is one parameter that is not determined. In general, it is the scattering angle. But it does not appear in the equation because we only integrated over the one-particle phase space in the production cross section. This information is lost and we have to reconstruct it. The notation is similar to the previous section. The Higgs four-momentum vector is given by the sum of the gluons momenta

$$p_H = p_1 + p_2 = x_1 P_1 + x_2 P_2 \tag{2.26}$$

which gives us the energy of the Higgs $E_H = (x_1 + x_2)E$. Here, E is the energy of a proton. We need to know this for the boost into the lab frame. In the center of mass frame, the decay of a Higgs boson is pretty easy to describe. The Higgs boson energy is only its mass and the momentum is zero. The two bottom quarks decay back-to-back because of momentum conservation and their energies are half the Higgs mass. Due to the Higgs boson that is spinless, there is no angle dependence in the decay. The bottom quark momenta are equally distributed on a sphere which means $\phi \in [0, 2\pi]$ and $\cos(\theta) \in [-1, 1]$ are generated by flat distributed random numbers. Thus, the four-momentum vector in the center of mass frame reads

$$p_b = \begin{pmatrix} \frac{m_H}{2} \\ p\sin(\theta)\cos(\phi) \\ p\sin(\theta)\sin(\phi) \\ p\cos(\theta) \end{pmatrix}, \quad p = \sqrt{\frac{m_H^2}{4} - m_b^2}\,. \tag{2.27}$$

But in general at the LHC, the Higgs boson will not be produced in the center of mass frame. This only happens when $x_1 = x_2$ is valid. For this reason, the bottom quark vector has to be boosted into the lab frame. This yields the vector

$$\begin{pmatrix} E_b \\ p_x \\ p_y \\ p_z \end{pmatrix} = \begin{pmatrix} \gamma & 0 & 0 & \gamma\beta \\ 0 & 1 & 0 & 0 \\ 0 & 0 & 1 & 0 \\ \gamma\beta & 0 & 0 & \gamma \end{pmatrix} \begin{pmatrix} \frac{m_H}{2} \\ p\sin(\theta)\cos(\phi) \\ p\sin(\theta)\sin(\phi) \\ p\cos(\theta) \end{pmatrix} \tag{2.28}$$

with

$$\beta = \sqrt{1 - \frac{m_H^2}{E_H^2}}, \quad \gamma = \frac{E_H}{m_H}\,. \tag{2.29}$$

If x_2 is bigger than x_1 then the boost must be performed in the negative z-direction, that means the sign of p_z flips. At this point, the event is completely generated and we can compute every physical quantity we want to simulate.

2.2.3. Algorithm for the program

The algorithm for calculating the total cross section and making the histograms for differential cross section is given by the following steps.

1. Set the limits of the physical observable
2. Set bin width
3. Repeat the following steps until sampling size is reached ($i < N$)
   a) Generate τ_i and y_i in the appropriate interval
   b) Evaluate the corresponding function at τ_i and y_i
   c) Generate an event
   d) Calculate the value of the observable in the lab frame
   e) Add the result of the function at τ_i and y_i to the corresponding bin of the observable value
4. Multiply every bin with $\frac{V}{N}$, where V is the integration volume
5. Calculate the total cross section by summing over all bins and multiplying with the bin width
6. Write histogram to a file

2.3. Results

In this section, we want to discuss the results I obtained from the program described above for the hadronic GF process in Fig. 2.2. The program determines the results numerically as described in Sec. 2.2.3. The parton distribution functions and the strong coupling constant are implemented with the LHAPDF (Les Houches Accord Parton Density Function) [32] interface to calculate the hadronic cross section. Via LHAPDF, we used the MRST2004 nlo [33] parametrization of the parton distribution functions. We embedded the RAN2 random

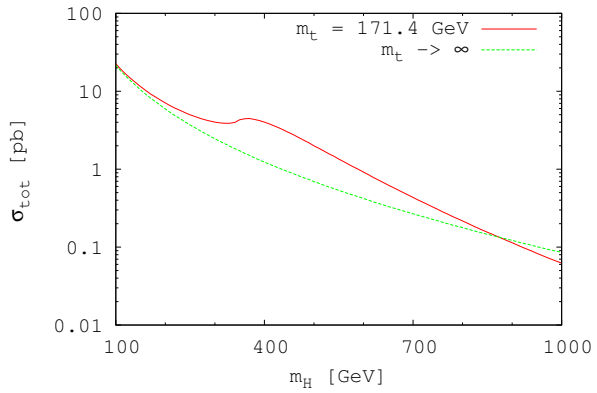

(a) Total cross section σ_{tot} of the GF Higgs production process in dependence of the Higgs mass m_H for finite and infinite top mass.

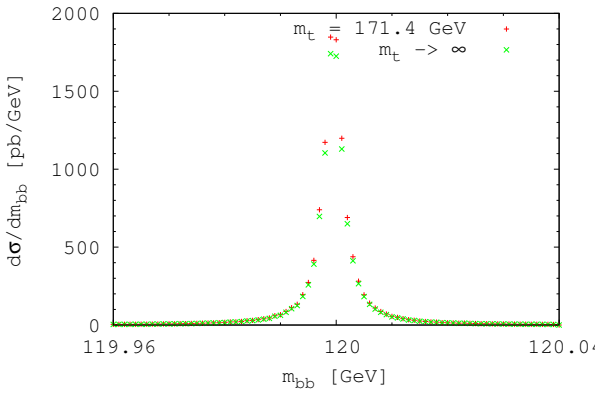

(b) Reconstruction of the invariant mass m_{bb} for a $m_H = 120\,\text{GeV}$ Higgs boson for finite and infinite top mass.

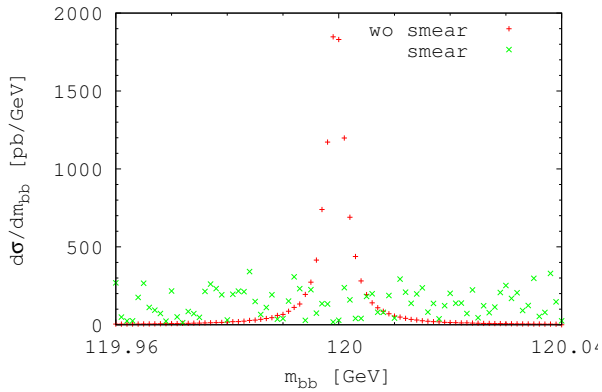

(c) Reconstruction of the invariant mass m_{bb} for a $m_H = 120\,\text{GeV}$ Higgs boson with and without detector effects

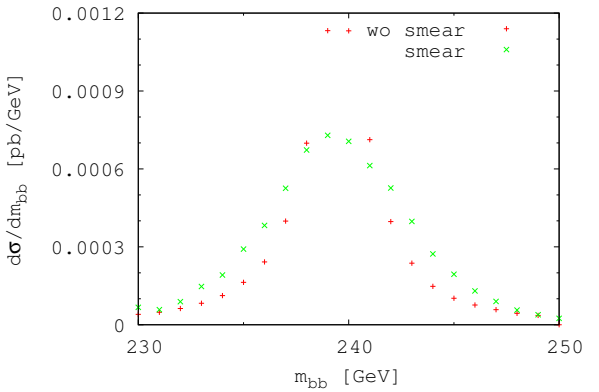

(d) Reconstruction of the invariant mass m_{bb} for a $m_H = 240\,\text{GeV}$ Higgs boson with and without detector effects

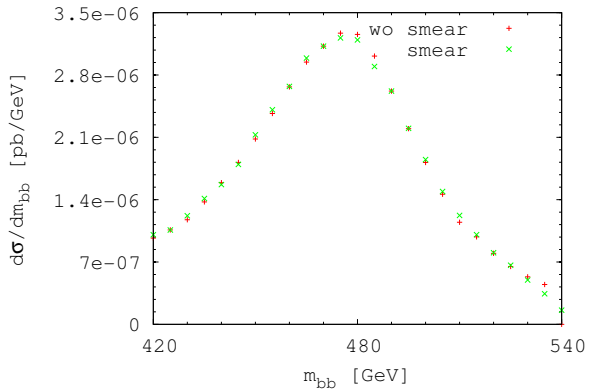

(e) Reconstruction of the invariant mass m_{bb} for a $m_H = 480\,\text{GeV}$ Higgs boson with and without detector effects

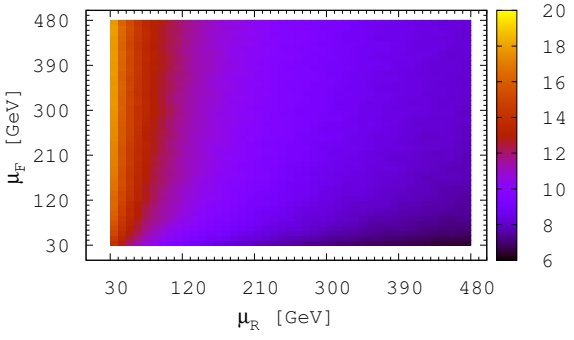

(f) The total cross section σ_{tot} in dependence of the renormalization μ_R and factorization scale μ_F

Figure 2.3.: The figures show the results for the total cross section in dependence of the Higgs mass and the factorization and renormalization scale, distribution of the invariant mass with and without simulated detector effects obtained from the MC program.

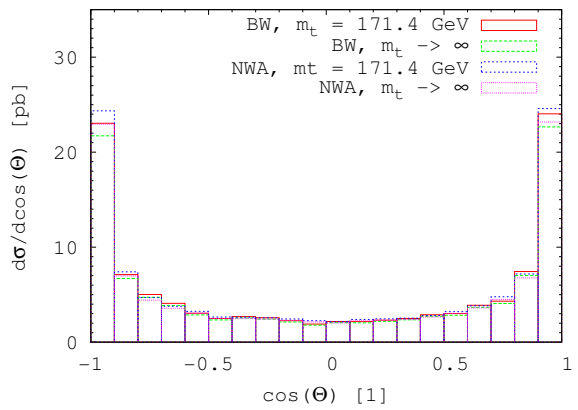

(a) $\cos(\theta)$ distribution in the lab frame

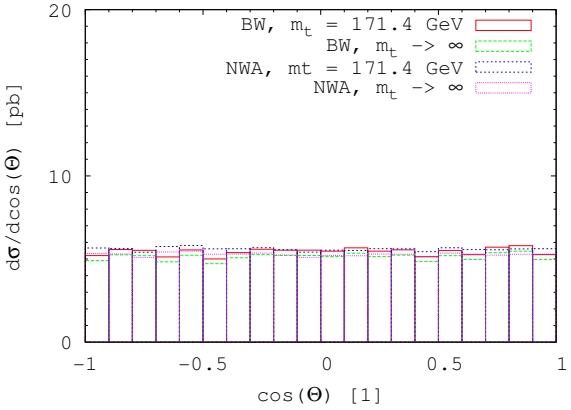

(b) $\cos(\theta)$ distribution in the com frame

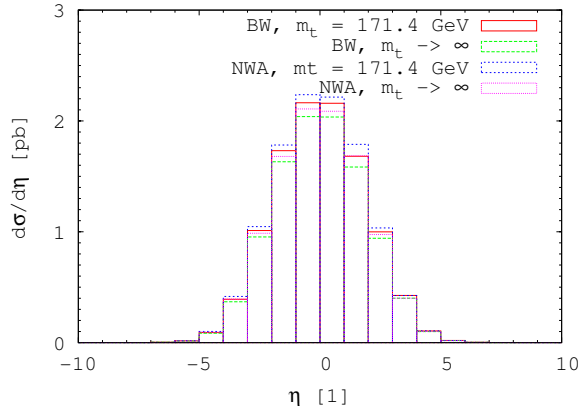

(c) Pseudorapidity distribution η in the lab frame

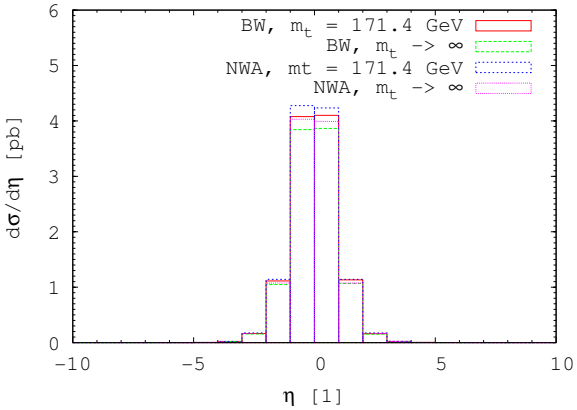

(d) Pseudorapidity distribution η in the com frame

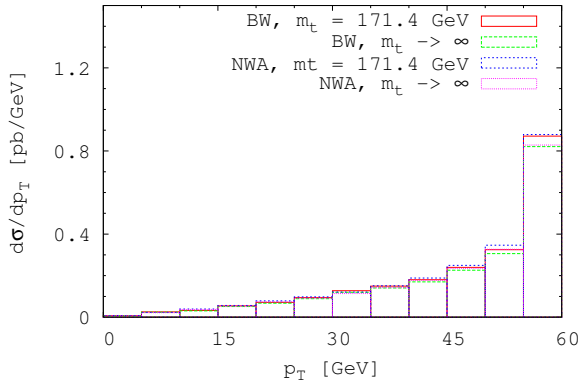

(e) Transverse momentum p_T distribution in the lab frame

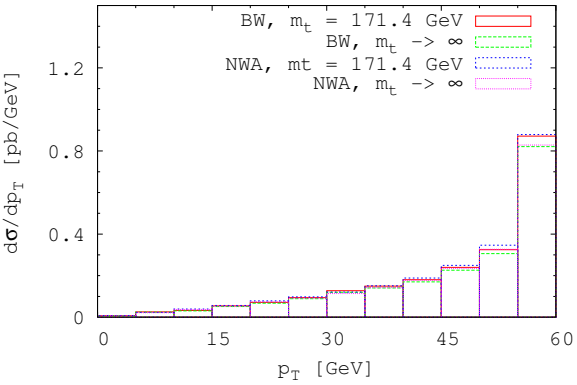

(f) Transverse momentum p_T distribution in the com frame

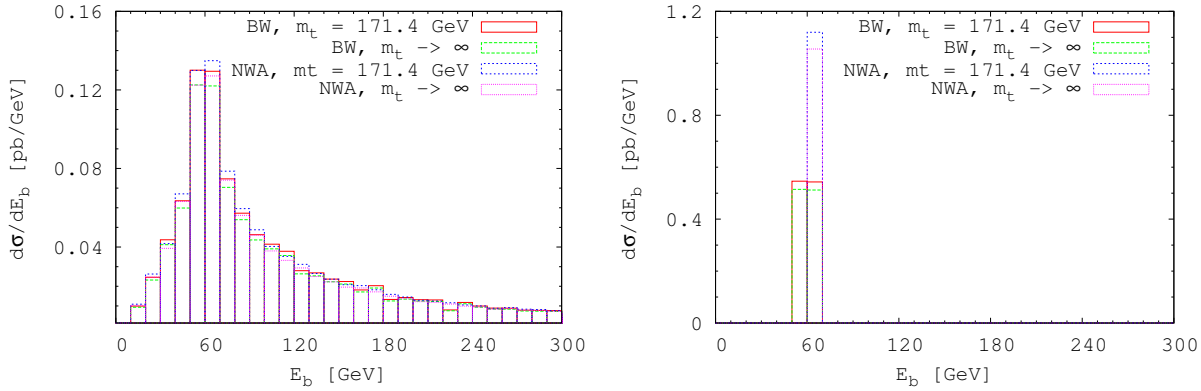

(g) Energy E_b distribution of one bottom-quark in lab frame

(h) Energy E_b distribution of one bottom-quark in com frame

Figure 2.4.: The figures show the distributions of observables measured from the bottom-quarks in the com and lab frame obtained from the MC program. Four different scenarios are compared. First the most realistic case where the Higgs mass is smeared out by a Breit-Wigner (BW) and with a finite top mass, second the BW with infinite top mass, third the narrow width approximation (NWA) with finite top mass and fourth the NWA with infinite top mass.

number generator from NUMERICAL RECIPES [51] in the program. The values for the top-quark mass $m_t = 171.4\,\text{GeV}$ and the bottom-quark mass $m_b = 4.2\,\text{GeV}$ are taken from the PARTICLE DATA GROUP [34].

Fig. 2.3(a) shows the total cross section σ_{tot} of the gluon-fusion Higgs production cross section for finite and infinite top-quark mass in dependence of the Higgs mass m_H. For the plot, 91 points are calculated each with a sampling size of 100000, that is a stepsize of ten GeV in the plotted range. In comparison with Ref. [52], there is a deviation of a global factor of roughly two. This is due to a K factor

$$K = \frac{\sigma_{HO}}{\sigma_{LO}} \tag{2.30}$$

that describes the deviation from higher order (HO) QCD corrections to the leading order (LO) process. In this work only leading order is taken into account. In the textbook [52], higher order of QCD corrections are taken into account. QCD corrections are in general big. Therefore, a factor of two can be identified with this. From this result, we know that the program delivers reasonable results.
In the total cross section there is bump for the finite top-quark case. The bump is located at twice the top mass because at that energy the top-quarks are produced on-shell. This leads to an enhancement of the cross section. In the infinite top-mass limit, the cross

section has no dependence of the top mass any more. Therefore, it cannot show this effect. The heavy top-quark limit is a good approximation for small Higgs masses.

In the Figs. 2.3(b)–2.3(e) the simulated invariant mass reconstruction from the bottom-quarks are shown. The reconstruction of the invariant mass is a common method at colliders to explore new particles, e.g., this was done for the Z-boson. From this measurement, one can conclude the mass of the particle and the total decay width. The Higgs boson is a highly unstable particle and decays in a very short period of time. Therefore, it cannot be seen directly in a detector. Only the decay products can be measured at colliders. From the measured energies and momenta of the decay products, the invariant mass of the intermediate particle can be reconstructed. The measurement of bottom-quarks is complicated at the LHC because of the huge QCD background. It is easier to detect charged leptons or photons where QCD does not play a role. The Higgs boson can decay either directly to charged leptons or via weak gauge bosons.
The first Fig. 2.3(b) depicts the comparison between a finite top-quark mass and the heavy top-quark limit. For a Higgs mass $m_H = 120\,\text{GeV}$, the error is rather small. In the above discussed total cross section, we saw that for small Higgs masses the heavy top-quark limit is a good approximation. For this reason the error here is expected to be small.

The next three figures show a simulation of the detector error for different Higgs masses (120 GeV, 240 GeV and 480 GeV). Because of the detector inaccuracy, the true value is smeared out by a Gaussian. The program first calculates the invariant mass m_{bb}^i and then determines a smeared value by a gauss distribution around that point with a standard deviation $\sigma = 0.01 m_{bb}^i$. For a small Higgs mass, this method for simulating the detector effect produces a much too big error. Therefore, no resonance for a light Higgs boson can be observed in Fig. 2.3(c) because of the huge noise. This method does not obtain a reasonable result and, for this reason, has to be improved. But for a bigger mass like $m_H = 240\,\text{GeV}$, see Fig. 2.3(d), show the qualitative right behavior: the higher peaked Breit-Wigner smears out to a flatter and broader Gauss distribution. For a $m_H = 480\,\text{GeV}$ the detector effect becomes smaller because of the bigger decay width, see Fig. 2.3(e).
The total decay width of the Higgs boson increases very strong around 160 GeV because the kinematic threshold for the W-boson is reach. At that stage, the Higgs boson can decay into two of these bosons on-shell. For Higgs masses bigger than that threshold, the branching ratio is dominated by this decay channel. For larger Higgs masses, the decay width is of the same order as its mass because of the longitudinal weak gauge bosons contribution.

In the following, we want to discuss the theory error for the cross section. The theory error arises from the strong coupling constant and the parton distribution function. The strong coupling constant depends on the energy scale that is called the renormalization scale μ_R. The running of the constant arises from loop correction in which divergences appear. Also the parton distribution function depends on the energy, called factorization scale μ_F. These two scales are not exactly determined at the scattering process. It is reasonable to assign these scales with the center of mass energy because it is an s-channel

μ_F [GeV]	μ_R [GeV]	σ_{tot} [pb]
30	30	14.35
30	480	6.18
480	30	18.98
480	480	8.19
120	120	11.11

Table 2.2.: Shows the total cross section of the four corners of Fig. (2.3(f)) and the reference point, when the two scales take the center of mass energy $E_{cm} = 120\,\text{GeV}$.

process. But it remains an uncertainty for these two parameters. Therefore it is better to scan the area around the center of mass energy to get a range in which the true value has to be expected. We chose the range $\frac{m_H}{4} \leq \mu_F, \mu_R \leq 4m_H$ and a step width of 10 GeV. According to this, 2116 points are calculated and the points between them are interpolated, see Fig. 2.3(f). In the following, the total cross section of all four corners of the figure are compared to the com energy because the deviation to these points are particularly big.

It shows that there is a huge deviation in the total cross sections σ_{tot}. From the upper left to lower right corner, see Tab. 2.3, there is a factor of more than three. And it makes an error of around 50%. The behavior in the renormalization scale is easy to see because there is an analytical expression for the running coupling constant

$$\alpha_S(\mu_R) = \frac{2\pi}{b_0 \log\left(\frac{\mu_R}{\Lambda}\right)} \tag{2.31}$$

which indicates that the coupling constant decreases with increasing energy.

In the following, we present the distributions for the cosine of the scattering angle θ, the pseudorapidity η, the transverse momentum p_T and the energy of the bottom quarks E_b for the four different cases: NWA and BW propagator with finite and inifite top-quark mass and compare the center of mass (com) and lab frame results. Every distribution is made with a sampling size of 100000.

We mentioned already that the Higgs has no spin. Hence, the decay product particles have no preferred direction. In the com frame we expect that $\cos(\theta)$ is flat. This is depicted in Fig. 2.4(b). The scattering angle is not Lorentz invariant. For this reason the distribution must be different in the lab frame, see Fig. 2.4(a). The Higgs boson decays in the lab frame. Thus, the quarks are boosted parallel or anti-parallel to the z-direction with equal likelihood. And hence, we expect that the scattering angle tends to 0 and π, which means peaks at $\cos(\theta) = \pm 1$.

The pseudorapidity η is defined by

$$\eta = \frac{1}{2} \log \left(\frac{1 + \cos(\theta)}{1 - \cos(\theta)} \right) . \tag{2.32}$$

It depends only on $\cos(\theta)$. If $\cos(\theta)$ is flat and symmetric, the η-distribution will be sharply peaked at $\eta = 0$ and will also be symmetric with respect to this point, see Fig. 2.4(d). In the lab frame Fig. 2.4(c), the peak flattens and broadens because $\cos(\theta)$ is shifted from the center to the outer part.

We next look at the transverse momentum distribution as a function of the transverse momentum. Because of the flatness of the $\cos(\theta)$ in the com frame, the propability for a bigger transverse momentum increases. This can be understood in the following way. If we slice the sphere where the quark momenta end such that the z-axis is cut perpendicularly and equidistantly then the area of the fraction of the sphere increases with increasing transverse momentum. The case where the transverse momentum is zero is very unlikely because it corresponds only to exactly two points of the surface (the intersection points with the z-axis). This explains the increase of the transverse momentum distribution for larger values. The transverse momentum is Lorentz invariant under boosts in the z-direction. Since, the distribution for the lab Fig. 2.4(e) and com frame Fig. 2.4(f) are identical. The transverse momentum of one bottom-quark cannot be bigger than half of the Higgs mass. This is because if Higgs boson decays such that the bottom-quark momentum is in the perpendicular direction to the z-axis the bottom-quark has the biggest transverse momentum. From Eq. (2.27) follows $p_T^{max} = \sqrt{m_H^2/4 - m_b^2}$. And as mentioned, the boost doesn't alter the result.

Finally, we look at the energy distribution as a function of the energy of one bottom-quark in the com Fig. 2.4(h) and lab frame Fig. 2.4(g). In the com frame, the energy is given by the Higgs mass such that both of the quarks takes half of it. Therefore, in this frame, it must be a sharp peak in the energy distribution at that point. But if the Higgs is not produced in resonance, the energy of the quarks smears out, too. For this reason, the energy splits into two bins.
In the lab frame, the energy distribution smears out to both sides because a bottom-quark can be boosted in the opposite direction, which lowers the momentum and thereby also the energy. The lowest energy a bottom-quark can have is its mass. The distribution has a peak at half the Higgs mass. that means that for most of the scattering events, the Higgs boson is not strongly boosted. The $\cos(\theta)$ and pseudorapidity distribution show a similar result. If most of the boost are very strong we would expect to see two peaks in the pseudorapidity distribution symmetrically located around $\eta = 0$ and stronger peaks in the $\cos(\theta)$ distribution.

In all subfigures of Fig. 2.3, the comparison of the four investigated scenarios shows rather small deviations. This has two main reasons. First, a 120 GeV Higgs boson has a very small decay width. For this reason, the Breit-Wigner distribution is sharply peaked and

therefore close to a Dirac delta function. Second, as mentioned before, the heavy top-quark limit is good if the mass is sufficiently big in comparison to the Higgs mass.

The MC program simulates the expected data for one special process at the LHC at a basic level. In most of the results no detector effects are considered. And the so far implemented detector effect is not good. No cuts on the events are taken into account. Cuts to the pseudorapidity and transverse momentum would give a more realistic picture. The beam pipe has a finite volume and therefore events with a small tranverse momentum cannot be measured.

This starting project, including the calculation of the gluon-fusion process, coding the program and applying it to that process, offered a good opportunity to get familiar with the techniques commonly used in LHC physics. In addition to this, it helped to get a better feeling for processes at the LHC and how to interpret the results which will be collected at the LHC.

3. Extensions of the Standard Model

In this section, we discuss two possible extensions to the Standard Model. First, we discuss a Higgs portal model, which is a kind of hidden valley model. Hidden valley models are present in supersymmetric models [35, 36] and String Theories [37]. Second, we discuss a composite Higgs model that arises from the breaking of a global symmetry where the Higgs boson is a pseudo Goldstone boson. These two models have in common, that they affect the Standard Model Higgs couplings by a fudge factor.

3.1. Hidden Higgs portal

There can be unknown particles in our universe because they are too heavy to be produced so far at colliders or there is a hidden valley which is accessible only via a heavy mediator belonging to the Standard Model. Hidden valley means that there is no connection to the already known Standard Model particles. At the moment, in the Standard Model exists a hypothetical sector that is the Higgs sector. The idea of a Higgs boson is more than four decades old, but the Higgs boson has not yet been observed. So it provides a good interface to get a link to a new physics sector.

Let us consider a hidden valley that consists of at least one gauge group with a corresponding Higgs boson. Also a complete copy of the Standard Model is possible, which means, the hidden sector would look like a mirror world [64]. The hidden Higgs boson is a singlet under the Standard Model gauge group $SU(3)_C \times SU(2)_L \times U(1)_Y$. To preserve renormalizability of the Standard Model also in the extended version, we consider only operators with mass dimension four in the Lagrangian. The new Langrangian looks like a copy of the Standard Model Higgs part and an additional interaction term between these Higgs bosons. It reads

$$-\mathscr{L} = \mu_s^2 |\phi_s|^2 + \lambda_s |\phi_s|^4 + \mu_h^2 |\phi_h|^2 + \lambda_h |\phi_h|^4 + \eta_x |\phi_s|^2 |\phi_h|^2 , \tag{3.1}$$

where s denotes the Standard Model and h the hidden sector. This kind of model is called Higgs portal [66].

3.1.1. Scalar case

First, we have a look at the simplest case where the prefactor of the quadratic hidden Higgs term is positive. In this case, the hidden Higgs does not acquire a vacuum expectation value v_h because the minimum of the potential is at the origin,

$$\mu_h^2 > 0 \quad \Rightarrow \quad v_h = 0\,; \tag{3.2}$$

therefore, the corresponding gauge group is not spontaneously broken by the Higgs or can be considered as an additional scalar to the Standard Model with a potential. Unitarity constraints for an ordinary additional scalar with a potential are discussed in Ref. [38]. And for the Standard Model Higgs follows

$$\mu_s^2 = -\lambda_s v_s^2\,, \tag{3.3}$$

the well known relation as in the minimal Standard Model Higgs version, so that the weak gauge group is still broken. This relation comes from the minium of the potential with the vacuum expectation value v_s. The basic idea of the Higgs mechanism is to introduce a complex $SU(2)$ doublet, which has four degrees of freedom. Three degrees of freedom are Goldstone bosons that break the gauge group and are eaten by the weak gauge bosons to give them the longitudinal polarization. The fourth degree of freedom is the Higgs boson. In the unitary gauge, the Standard Model and the hidden Higgs field become

$$\phi_s = \begin{pmatrix} 0 \\ \frac{v_s + h_s}{\sqrt{2}} \end{pmatrix}, \quad \phi_h = \frac{h_h}{\sqrt{2}}\,. \tag{3.4}$$

Putting this into Eq. (3.1), the expanded Langrangian is given by

$$\begin{aligned} -\mathscr{L}_s &= \frac{\mu_s^2}{2}\left(v_s^2 + 2v_s h_s + h_s^2\right) + \frac{\lambda_s}{4}\left(v_s^4 + 4v_s^3 h_s + 6v_s^2 h_s^2 + 4v_s h_s^3 + h_s^4\right)\,, \\ -\mathscr{L}_h &= \frac{\mu_h^2}{2} h_h^2 + \frac{\lambda_h}{4} h_h^4\,, \\ -\mathscr{L}_x &= \frac{\eta_x}{4}\left(v_s^2 + 2v_s h_s + h_s^2\right) h_h^2\,. \end{aligned} \tag{3.5}$$

Sorting the Lagrangian by the powers of the fields helps to read off the masses and the interactions among the fields:

$$\begin{aligned}
-\mathscr{L}_{mass} &= \frac{1}{2}\left(\mu_s^2 + 3\lambda_s v_s^2\right) h_s^2 + \frac{1}{2}\left(\mu_h^2 + \frac{\eta_x v_s^2}{2}\right) h_h^2\,, \\
-\mathscr{L}_{int} &= \frac{\eta_x}{4} h_s^2 h_h^2 + \frac{\eta_x}{2} v_s h_s h_h^2\,, \\
-\mathscr{L}_{self} &= \frac{\lambda_s}{4} h_s^4 + \lambda_s v_s h_s^3 + \frac{\lambda_h}{4} h_h^4\,, \\
-\mathscr{L}_{const} &= \frac{\lambda_s}{4} v_s^4 + \frac{\mu_s^2}{2} v_s^2\,.
\end{aligned} \tag{3.6}$$

While the mass term is not affected by the hidden sector and remains the same as in the minimal Standard Model, the mass term of the hidden Higgs depends on the Standard Model vacuum expectation value v_s and the coupling constant of the interaction term χ_x.

$$m_s^2 = \mu_s^2 + 3\lambda_s v_s^2 = 2\lambda_s v_s^2\,, \qquad m_h^2 = \mu_h^2 + \frac{\eta_x v_s^2}{2}\,. \tag{3.7}$$

We can forget about the constant Lagrangian above because the physics is in the equations of motion, which are given by derivatives of the Lagrangian. Also the Standard Model Higgs interactions remains unaffected but are extended by a four-point self-interaction of the hidden Higgs boson and a four- and three-point interaction term between the SM and hidden Higgs boson.

The electroweak sector of the model consists of two gauge groups. The first group, the $SU(2)_L$, has three generators $T^a = \frac{\tau^a}{2}$, where τ are the Pauli matrices and the three corresponding fields W_μ^a. The second group, $U(1)_Y$, has only one generator and therefore only one corresponding field B_μ. The Standard Model Higgs doublet is charged under the $U(1)_Y$ with hypercharge $Y = 1$. Because of this, it couples to both groups via the covariant derivative,

$$\begin{aligned}
|D_\mu \Phi_s|^2 =& \left| \left(\partial_\mu - \mathrm{i} g_2 \frac{\tau_a}{2} W_\mu^a - \mathrm{i} g_1 \frac{1}{2} B_\mu\right) \Phi_s \right|^2 \\
=& \frac{1}{2}(\partial_\mu h_s)^2 + \frac{1}{8} g_2^2 \left(v_s + h_s\right)^2 \left|W_\mu^1 + \mathrm{i} W_\mu^2\right|^2 + \frac{1}{8}\left(v_s + h_s\right)^2 \left|g_2 W_\mu^3 - g_1 B_\mu\right|^2 \\
=& \frac{1}{2}(\partial_\mu h_s)^2 + m_W^2 W_\mu^+ W^{-\mu} + \frac{1}{2} m_Z^2 Z_\mu Z^\mu \\
&+ \frac{2m_W^2}{v_s} h_s W_\mu^+ W^{-\mu} + \frac{m_Z^2}{v_s} h_s Z_\mu Z^\mu + \frac{m_W^2}{v_s^2} h_s^2 W_\mu^+ W^{-,\mu} + \frac{m_Z^2}{2v_s^2} h_s^2 Z_\mu Z^\mu\,,
\end{aligned} \tag{3.8}$$

where g_1 and g_2 denote the coupling constants to the two gauge groups. With the definitions of the mass eigenstates

$$W_\mu^\pm = \frac{1}{\sqrt{2}}\left(W_\mu^1 \mp \mathrm{i}W_\mu^2\right) , \quad Z_\mu = \frac{g_2 W_\mu^3 - g_1 B_\mu}{\sqrt{g_1^2+g_2^2}} , \quad A_\mu = \frac{g_2 W_\mu^3 + g_1 B_\mu}{\sqrt{g_1^2+g_2^2}} , \tag{3.9}$$

and the masses

$$m_W = \frac{1}{2} g_2 v_s, \quad m_Z = \frac{1}{2}\sqrt{g_1^2+g_2^2}\, v_s , \tag{3.10}$$

the Langrangian of Eq. (3.8) yields the kinetic term of the Higgs boson, the coupling to the weak gauge bosons and their mass terms. The $SU(2)$ is broken and $U(1)$ remains unbroken with the field A_μ that can be identified with the photon. The charged weak gauge bosons are complex fields; therefore, it makes a difference of a factor two to the neutral gauge boson terms.

At this point we achieved our first goal. We have derived the mass terms of the weak gauge bosons. Our second goal, determining the fermion mass term, is still left. The weak interaction distinguishes between left- and right-handed particles. The W-boson couples only to left-handed particles and transforms an up-type fermion to a down-type fermion and vice versa. Due to the coupling only to left-handed particles, the weak interaction violates maximally parity. The W-boson couples to all fermions with the same strength except of the quarks because of the Cabibbo rotation. This leads to a small correction to the quark couplings. For the Z-boson, the situation is different because its couplings to the fermions are charge dependent. Thus, the left-handed particles are doublets under the $SU(2)$,

$$L \in \left\{ \begin{pmatrix} \nu_e \\ e \end{pmatrix}_L , \begin{pmatrix} \nu_\mu \\ \mu \end{pmatrix}_L , \begin{pmatrix} \nu_\tau \\ \tau \end{pmatrix}_L \right\} , \quad Q \in \left\{ \begin{pmatrix} u \\ d \end{pmatrix}_L , \begin{pmatrix} c \\ s \end{pmatrix}_L , \begin{pmatrix} t \\ b \end{pmatrix}_L \right\} , \tag{3.11}$$

and the right-handed fermions are singlets,

$$e \in \{e_R, \mu_R, \tau_R\} , \quad u \in \{u_R, c_R, t_R\} , \quad d \in \{d_R, s_R, b_R\} . \tag{3.12}$$

Leptons and quarks can be grouped into three generations. Because of the handedness, a Dirac mass term $\mathscr{L} = -m(\bar{\Psi}_L \Psi_R + \bar{\Psi}_R \Psi_L)$ is forbidden in order to preserve gauge invariance. The Higgs doublet can solve this problem. The mass terms are given by Yukawa couplings

$$\begin{aligned} \mathscr{L}_F &= -\lambda_e^i \bar{L}_i \Phi_s e_i - \lambda_d^i \bar{Q}_i \Phi_s d_i - \lambda_u^i \bar{Q}_i \tilde{\Phi}_s u_i + h.c. \\ &= -\frac{1}{\sqrt{2}} \lambda_e \left(v_s + h_s\right) \bar{e}_L e_R - \frac{1}{\sqrt{2}} \lambda_d \left(v_s + h_s\right) \bar{d}_L d_R - \frac{1}{\sqrt{2}} \lambda_u \left(v_s + h_s\right) \bar{u}_L u_R + \cdots , \end{aligned} \tag{3.13}$$

where $\tilde{\Phi}_s = \mathrm{i}\tau_2\Phi^*$ is the isodoublet, has hypercharge $Y = -1$ and gives the mass to the up-type quarks. In the first line of Eq. (3.13), the index i implies a summation over the three generations, and in the second line, only the first generation is shown in full detail. The Lagrangian in Eq. (3.13) describes two things. First, the mass term of the fermions with mass

$$m_f = \frac{\lambda_f v_s}{\sqrt{2}}\,, \tag{3.14}$$

which is proportional to the vacuum expectation value v_s, and second, the coupling of the Higgs boson to the fermions. In this model, the neutrinos are still massless. And there is another weak point in the model. Instead of the fermion mass m_f, the Yukawa coupling constant λ_f has to be put into the theory.

As we have seen, the hidden Higgs boson only couples directly to the Higgs boson of the Standard Model and can affect the total decay width if

$$m_s > 2m_h \tag{3.15}$$

is valid. Then additional invisible decays to the hidden valley are possible. And with that, the branching ratios of the decay channels decreases. In the scalar case, the Standard Model Higgs couplings are still unaffected. The hidden Higgs boson can only have effects on the Standard Model via higher order corrections, not until at two loop order.

3.1.2. Mixing case

In the following, we explain the more general case, in which both Higgs bosons acquire a vacuum expectation value, and implications to the Standard Model. Analogous to the scalar case, all the steps have to be done again. The Standard Model Higgs remains as in Eq. (3.4) but the hidden Higgs now reads

$$\phi_h = \frac{v_h + h_h}{\sqrt{2}}\,. \tag{3.16}$$

Putting this into Eq. (3.1) and using

$$\begin{aligned}
\frac{\partial V}{\partial \left|\Phi_s\right|^2} &= \mu_s^2 + 2\lambda_s \left|\Phi_s\right|^2 + \eta_x \left|\Phi_h\right|^2 = 0 \quad \Rightarrow \quad \mu_s^2 = -\lambda_s v_s^2 - \frac{\eta_x}{2} v_h^2 \\
\frac{\partial V}{\partial \left|\Phi_h\right|^2} &= \mu_h^2 + 2\lambda_h \left|\Phi_h\right|^2 + \eta_x \left|\Phi_s\right|^2 = 0 \quad \Rightarrow \quad \mu_h^2 = -\lambda_h v_h^2 - \frac{\eta_x}{2} v_s^2\,,
\end{aligned} \tag{3.17}$$

where $V = -\mathscr{L}$ is the potential, yields the Lagrangians

$$\begin{aligned} -\mathscr{L}_{mass} &= \lambda_s v_s^2 h_s^2 + \eta_x v_s v_h h_s h_h + \lambda_h v_h^2 h_h^2 \,, \\ -\mathscr{L}_{int} &= \frac{\eta_x}{4} h_s^2 h_h^2 + \frac{\eta_x}{2} v_h h_s^2 h_h + \frac{\eta_x}{2} v_s h_s h_h^2 \,, \\ -\mathscr{L}_{self} &= \frac{\lambda_s}{4} h_s^4 + \lambda_s v_s h_s^3 + \frac{\lambda_h}{4} h_h^4 + \lambda_h v_h h_h^3 \,, \\ -\mathscr{L}_{const} &= -\frac{\lambda_s}{4} v_s^4 - \frac{\eta_x}{4} v_s^2 v_h^2 - \frac{\lambda_h}{4} v_h^4 \,. \end{aligned} \tag{3.18}$$

At this point, the mass term looks interesting because of the second summand which is proportional to the product of the two Higgs bosons. This indicates a mass mixing of the two bosons. The next step is to calculate the mass eigenstates; this is done in App. C. The mass mixing matrix is symmetric; therefore, it has real eigenvalues which are the masses of the mass eigenstates m_1 and m_2. To the eigenvalues correspondsorthogonal eigenvectors. Thus, the mass eigenstates h_1 and h_2 can be written as

$$\begin{pmatrix} h_1 \\ h_2 \end{pmatrix} = \begin{pmatrix} \cos\chi & \sin\chi \\ -\sin\chi & \cos\chi \end{pmatrix} \begin{pmatrix} h_s \\ h_h \end{pmatrix} \,, \tag{3.19}$$

where χ is the mixing angle. For small mixing angles, h_1 is a SM-like Higgs boson. Putting the mass eigenstates into Eq. (3.18), we get the mass Lagrangian

$$-\mathscr{L}_{mass} = \frac{1}{2} \begin{pmatrix} h_1 \\ h_2 \end{pmatrix}^T \begin{pmatrix} m_1^2 & 0 \\ 0 & m_2^2 \end{pmatrix} \begin{pmatrix} h_1 \\ h_2 \end{pmatrix} = \frac{1}{2} m_1^2 h_1^2 + \frac{1}{2} m_2^2 h_2^2 \tag{3.20}$$

and all the possible interaction terms

$$\begin{aligned} -\mathscr{L}_{int} &= \frac{1}{2}\eta_{112} h_1^2 h_2 + \frac{1}{2}\eta_{122} h_1 h_2^2 + \frac{1}{4}\eta_{1112} h_1^3 h_2 + \frac{1}{4}\eta_{1222} h_1 h_2^3 \\ -\mathscr{L}_{self} &= \frac{1}{2}\eta_{111} h_1^3 + \frac{1}{2}\eta_{222} h_2^3 + \frac{1}{4}\eta_{1111} h_1^4 + \frac{1}{4}\eta_{2222} h_2^4 \,. \end{aligned} \tag{3.21}$$

In this scenario a lot of possible interaction terms appear. The coupling constants η are written down explicitly in App. D and all the Feynman rules are shown there as well.

To see how the mass eigenstates affect the couplings to the weak gauge bosons, we need to put them into Eq. (3.8). Then, it follows

$$
\begin{aligned}
|D_\mu \Phi_s|^2 \propto & \frac{2m_W^2}{v_s} c_\chi h_1 W_\mu^+ W^{-\mu} + \frac{m_Z^2}{v_s} c_\chi h_1 Z_\mu Z^\mu + \frac{m_W^2}{v_s^2} c_\chi^2 h_1^2 W_\mu^+ W^{-\mu} + \frac{m_Z^2}{2v_s^2} c_\chi^2 h_1^2 Z_\mu Z^\mu \\
& - \frac{2m_W^2}{v_s^2} c_\chi s_\chi h_1 h_2 W_\mu^+ W^{-\mu} - \frac{m_Z^2}{v_s^2} c_\chi s_\chi h_1 h_2 Z_\mu Z^\mu \\
& - \frac{2m_W^2}{v_s} s_\chi h_2 W_\mu^+ W^{-\mu} - \frac{m_Z^2}{v_s} s_\chi h_2 Z_\mu Z^\mu + \frac{m_W^2}{v_s^2} s_\chi^2 h_2^2 W_\mu^+ W^{-\mu} + \frac{m_Z^2}{2v_s^2} s_\chi^2 h_2^2 Z_\mu Z^\mu
\end{aligned}
\tag{3.22}
$$

with $c_\chi = \cos\chi$ and $s_\chi = \sin\chi$. From this equation, we can read off two things. First, the couplings are affected by the mixing angle, and second, both Higgs bosons couple to the weak gauge bosons. The kinetic terms of the Higgs bosons come from the sum of the two covariant derivatives, one, D_μ, acting on the Standard Model doublet and and another, D'_μ, acting on the hidden Higgs field

$$
|D_\mu \Phi_h|^2 + \left|D'_\mu \Phi_h\right|^2 \propto \frac{1}{2} \left(\partial_\mu h_1\right)^2 + \frac{1}{2} \left(\partial_\mu h_2\right)^2 . \tag{3.23}
$$

From the Yukawa couplings to fermions in Eq. (3.13) results

$$
\mathscr{L}_F = -\frac{1}{\sqrt{2}} \lambda_e \left(v_s + c_\chi h_1 - s_\chi h_2\right) \bar{e}_L e_R + \cdots . \tag{3.24}
$$

Only the coupling to electron is shown. The mass term is not influenced by the hidden Higgs but the couplings are affected by the mixing angle, too. Because of the mass mixing, the mass eigenstates are linear combinations of the two Higgs fields. Through the SM-component, the mass eigenstates couple to the Standard Model particles. For this reason, the couplings are affected by the mixing angle. But this modification of the couplings is the same for every kind of particle. This means that the modification due to the mixing is universal. Also the cross sections and decay widths are modified by this factor. Because of decays to the hidden sector, additional invisible decay modes are possible which increase the total decay width as well. We will have a closer look at this in Sec. 4.1.

The mass mixing makes it possible that both Higgs bosons can couple to both sectors. Therefore, also the hidden Higgs field couples to the weak gauge bosons. This can affect the Peskin-Takeuchi parameters which describe the electroweak radiative corrections. From further investigations of this impact, probably any constraints to the parameters of the hidden Higgs portal model can be derived.

3.2. Minimal composite Higgs model

The general idea of a composite Higgs boson is several decades old. At the beginning, people thought about a Higgs boson as a quark condensate in analogy to a meson or baryon. In this case, the electroweak symmetry is broken by QCD. Because of the relation to QCD, such kind of model is called technicolor. In contrary to an elementary scalar particle, the composite Higgs boson does not have quadratic divergences, that means, it is natural and therefore the hierarchy problem does not appear. In the most basic concept, Technicolor can give a mass to the weak gauge bosons. But to give the fermions a mass an extension is needed. In the extended version, additional gauge interactions are introduced. Technicolor models that are based on QCD face a problem. They contradict electroweak precision data, by predicting wrong masses for the gauge bosons, and constraints of neutral flavor-changing current.

A solution to this problem is to introduce a new strong dynamic that breaks a global symmetry. Then, the composite Higgs boson arises as a pseudo-Goldstone boson. In the last decade, such an approach with the interplay of models with extra dimensions, like the Randall-Sundrum model, became popular. In the Randall-Sundrum model [22], the universe is a five dimensional anti de Sitter space. An anti de Sitter space is a space with negative curvature, e.g. a hyperbolic space. Along the additional space dimension y, two branes (3+1 dimensional subspace) are located at $y = 0$, that is the ultraviolet (UV) brane where the fields of the Standard Model live, and at $y = L$, the infrared (IR) brane. The empty space between this two branes along the extra dimension is the so-called bulk. The new composite sector is located in the five dimensional bulk and IR brane. The AdS/CFT correspondence [23] makes it possible to map a strongly-coupled four dimensional theory to a weakly-coupled theory in five dimensions.

The minimal composite Higgs model (MCHM) that we also consider in our Higgs couplings analysis in Sec. 4.2 is based on the strong-interacting light Higgs (SILH) model. The effective Lagrangian of the SILH model includes higher dimensional operators [75]

$$\begin{aligned}\mathscr{L}_{SILH} =& \frac{c_H}{2f^2}\left(\partial_\mu |H|^2\right)^2 + \frac{c_T}{2f^2}\left(H^\dagger D_\mu H\right)^2 - \frac{c_6\lambda}{f^2}|H|^6 + \left(\frac{c_y y_f}{f^2}|H|^2\,\bar{f}_L H f_R + h.c.\right) \\ &+ \frac{\mathrm{i}c_w g}{2m_\rho^2}\left(H^\dagger\sigma^i D^\mu H\right)\left(D^\nu W_{\mu\nu}\right)^i + \frac{\mathrm{i}c_B g'}{2m_\rho^2}\left(H^\dagger D^\mu H\right)\left(\partial^\nu B_{\mu\nu}\right) \\ &+ \frac{\mathrm{i}c_{HW} g}{16\pi^2 f^2}\left(D^\mu H\right)^\dagger\sigma^i\left(D^\nu H\right)W^i_{\mu\nu} + \frac{\mathrm{i}c_{HB} g'}{16\pi^2 f^2}\left(D^\mu H\right)^\dagger\left(D^\nu H\right)B_{\mu\nu} \\ &+ \frac{c_\gamma g'^2}{16\pi^2 f^2}\frac{g^2}{g_\rho^2}|H|^2 B_{\mu\nu}B^{\mu\nu} + \frac{c_g g_S^2}{16\pi^2 f^2}\frac{y_t^2}{g_\rho^2}|H|^2 G^a_{\mu\nu}G^{a\mu\nu}\,,\end{aligned} \tag{3.25}$$

where g, g' and g_S denote the Standard Model electroweak gauge couplings and the strong coupling, y_f is the SM Yukawa coupling to the fermions $f_{L,R}$, λ is the SM quartic Higgs coupling, c_x are coefficients of order one unless protected by some symmetry, $W_{\mu\nu}$, $B_{\mu\nu}$ and $G_{\mu\nu}$ are the field strength tensors of the Standard Model, f is the scale of the Goldstone boson of the strong sector, m_ρ is the mass scale of the new resonances with their coupling g_ρ, and D is the covariant derivative. The first line of Eq. (3.25) will affect the physics of the Higgs boson and will cause a shift in the Higgs couplings. The first and fourth term of that line give the major contribution to this effect. The second term leads to a correction to the ρ-paramter, $\Delta\rho = c_T\xi$, which has a strong constraint from LEP precision data. The last three lines of Eq. (3.25) will act as form factors. The second last line is one-loop suppressed and the last line is more than one-loop suppressed. The last line affects directly the gluon-fusion Higgs production and the Higgs decay to photons.

We assume that the bulk gauge symmetry is $SO(5) \times U(1) \times SU(3)$ and that it is broken down to the Standard Model gauge group on the UV brane and to $SO(4) \times U(1) \times SU(3)$ on the IR brane. The $SO(5)$ has ten generators and the $SO(4)$ has six generators. If the $SO(5)$ is broken down to an $SO(4)$ then four Goldstone bosons appear. The Goldstone bosons can be parameterized by the $SO(5)/SO(4)$ coset [125]

$$\Sigma = \langle\Sigma\rangle \exp\left(\frac{\Pi}{f}\right) \quad \langle\Sigma\rangle = \begin{pmatrix}0, & 0, & 0, & 0, & 1\end{pmatrix} \quad \Pi = -\mathrm{i}T^a h^a \sqrt{2} = \begin{pmatrix} 0_4 & H \\ -H^T & 0 \end{pmatrix}, \tag{3.26}$$

where T^a are the four broken generators and h^a the corresponding Goldstone bosons. In the unitary gauge, Σ becomes

$$\Sigma = \begin{pmatrix}\sin\frac{h}{f}, & 0, & 0, & 0, & \cos\frac{h}{f}\end{pmatrix}. \tag{3.27}$$

At this stage, we are able to derive the kinetic term of the Higgs boson and its interaction with the weak gauge bosons. It reads

$$\begin{aligned}\mathscr{L}_{kin} =& \frac{f^2}{2}\left(D_\mu \Sigma\right)^2 \\ =& \frac{1}{2}\left(\partial_\mu h\right)^2 + m_W^2(h)\left(W_\mu W^\mu + \frac{1}{2\cos^2\theta_W} Z_\mu Z^\mu\right)\end{aligned} \tag{3.28}$$

with the W-boson mass

$$m_W(h) = \frac{gf}{2}\sin\frac{h}{f}. \tag{3.29}$$

In this model, the coupling constants from the Higgs boson are modified in comparison to the minimal Standard Model

$$g_{HVV} = g_{HVV}^{SM}\sqrt{1-\xi} \quad g_{HHVV} = g_{HHVV}^{SM}\left(1-2\xi\right) , \tag{3.30}$$

where ξ is the compositeness parameter that is given by

$$\xi = \left(\frac{v}{f}\right)^2 = \sin^2\frac{\langle h\rangle}{f} . \tag{3.31}$$

The compositeness parameter interpolate between two schemes, which are the Standard Model ($\xi = 0$) and Technicolor ($\xi = 1$). In the last step, we have to figure out how the fermion couplings are affected. The modification of the couplings to the fermions depends on the embedding of the Standard Model fermions into the representation of the bulk symmetry.

3.2.1. MCHM4

First, the fermions can transform under the spinorial representation of the $SO(5)$ [125]. Then, the Yukawa couplings of the fermions to the Higgs boson has the form

$$\mathscr{L}_{yuk} = -m_f\left(h\right)\bar{f}f , \quad m_f\left(h\right) = M\sin\frac{h}{f} , \tag{3.32}$$

This leads to a shift in the couplings

$$g_{Hff} = g_{Hff}^{SM}\sqrt{1-\xi} . \tag{3.33}$$

This realization of the fermions leads to the same modification in the couplings as to the weak bosons.

3.2.2. MCHM5

Second, the fermions can transform under the fundamental representation of the $SO(5)$ [126]. The fermion Higgs boson interaction part then reads

$$\mathscr{L}_{yuk} = -m_f\left(h\right)\bar{f}f , \quad m_f\left(h\right) = M\sin\frac{2h}{f} . \tag{3.34}$$

This Lagrangian causes a different modification in the Yukawa couplings, which reads

$$g_{Hff} = g_{Hff}^{SM} \frac{1-2\xi}{\sqrt{1-\xi}} \,. \tag{3.35}$$

In this case, the Higgs boson couplings to the fermions and vector bosons are affected differently and therefore the modifications are partially universal.

In both models the modifications to the vector bosons are the same. The couplings are reduced in comparison to the Standard Model. While the MCHM4 shows the same behavior for the fermions, the MCHM5 has some new features. For small values of ξ, MCHM5 shows qualitatively a similar behavior. But for $\xi = 0.5$ the fermion couplings vanish and for large ξ the couplings are getting bigger than the SM-couplings. This effect can significantly effect the Higgs search.

4. Measuring hidden Higgs and strongly-interacting Higgs scenarios

As we have seen in Chap. 3, there are models that extend the Standard Model (SM) and have an impact on the Higgs couplings predicted from the minimal Higgs sector of the Standard Model [54–61]. In this chapter we want to investigate these models with the SFitter program and discuss the results. From measuring the Higgs couplings at the LHC [62, 63], we can get a better understanding of potential scenarios beyond the Standard Model. Let us summarize the two well motivated models for which the analysis is particularly transparent.

1. There are models beyond the Standard Model which can have a hidden sector. The hidden sector can contain a Higgs that breaks a gauge group there. The Higgs boson is a good candidate for a mediator to open the portal to the hidden sector [64–71] because the Higgs boson is not observed yet. Therefore the hidden sector cannot be observed so far. The coupling between the SM-singlet Higgs mass term and the corresponding SM-neutral Higgs term in the hidden sector leads to an interaction which transfer the renormalizability from the Standard Model to the entended theory.

2. In the minimal Higgs sector of the Standard Model, the Higgs boson is an elementary particle like an electron and therefore pointlike. From the breaking of a global symmetry it is thinkable that the Higgs boson is a composite pseudo-Goldstone boson caused by new strong interactions. These models are well motivated scenario [72–79] as well.

If there is a hidden Higgs sector that is linked to the Standard Model via the Higgs boson, the couplings to the Standard Models particles are modified because of the mixing of the two Higgs bosons. These modification is the same to all particles and therefore universally. This leads to a deviation in the decay width and cross sections. Because of the presence of the hidden sector, in this model, further invisible decays are possible. Invisible decays means, that the decay products cannot be measured in the detectors, like neutrinos in the Standard Model, because of their weakly interacting behaviour. These additional invisible decays also affect the total decay width. In strongly interacting models where the Higgs boson emerges as a pseudo-Goldstone boson the modifications of the couplings are dependent on the specific model. In the MCHM4 model the couplings and therefore the cross sections and decay width are affected universally as well as the hidden Higgs

model. In contrary, the MCHM5 model predicts differect modification of the couplings depending on the type of particles. Couplings to fermions are affected in a different way than bosons. For this reason the modification is partially universal. These kind of models do not predict any new invisible decays. For this reason, the set of characteristics will allow us to distinguish between the wo scenarios.

In general, depending on the operator basis chosen [80–94], some $\mathcal{O}(10)$ free parameters may affect the measured production and decay rates at the LHC. A universal (or partially universal) modification of the Higgs couplings tremendously simplifies the complexity of any experimental analysis to the measurement of just one, or two, new parameters. Furthermore, setting bounds on universal deviations from the Standard Model Higgs couplings measures the degree of concordance between the observed Higgs boson and the Standard Model in a particularly transparent form.

In the two scenarios introduced above, the twin width-ratios of the Higgs boson are modified by a parameter κ:

$$\frac{\Gamma_p \Gamma_d}{\Gamma_{tot}} = \kappa \left(\frac{\Gamma_p \Gamma_d}{\Gamma_{tot}} \right)^{\text{SM}} . \tag{4.1}$$

The partial widths refer to the production channel p and the decay mode d, either exclusively or summing over sets of initial or final states. These ratios are measured, at the Born level, directly by the product of production cross section times decay branching ratio of the process $p \to Higgs \to d$ in the narrow width approximation. That means the cross section for the whole process splits into the production cross section times the branching ratio of the decay mode, see Sec. 2.1.2 . In the hidden sector the parameter κ is universal; in the strong interaction scenario we consider it may take different values for Higgs couplings to vector bosons or fermions [79].

For a hidden sector the decay label d includes invisible Higgs decays, *i.e.* the partial width Γ_{hid}. This second parameter can be measured via the invisible branching ratio BR_{inv}. It is well-known [95–99] that the determination of BR_{inv} at hadron colliders is quite demanding, even through it naturally appears in many extensions of the Standard Model, like four lepton generations or supersymmetry [71]

In the present study we will show, adopting the tools of SFitter, at which level κ as well as Γ_{hid}, if present, can be determined at the LHC.

The measurements of κ and BR_{inv} do not require the estimate of the total width appearing in the denominator of Eq. (4.1). Nevertheless, estimating Γ_{tot} will provide us with consistency checks on our theoretical ansatz. One way is to simply identify the total Higgs width with the sum of all partial widths, with or without invisible channels [63]. The non-observed partial widths are fixed to the Standard Model value scaled by the same global factor applied to the observed partial widths. This method relies strongly on the

recent resurrection of the $H \to b\bar{b}$ channel based on fat jet searches [100–102]. An alternative way to construct an upper limit to the Higgs width — to be combined with the lower limit from all observed partial widths — would be motivated by the unitarization of $WW \to WW$ scattering. The Standard Model Higgs state saturates this unitarization, so modulo quantum corrections the relation $g_{WWH} \lesssim g^{\text{SM}}_{WWH}$ becomes an upper bound to the Higgs width [62]. We cannot use such an additional constraint because the observed scalar state in our models overlaps only partly with the state related to electroweak symmetry breaking.

Extracting Higgs parameters from LHC data [62, 63] forces us to pay attention to the different uncertainties affecting the rate measurements and their comparison to theory predictions for Higgs production [103–117] and decay [118, 119]. For typical luminosities around 30 fb^{-1} statistical uncertainties will be the limiting factor for example in weak-boson-fusion or Higgs-strahlung channels. Simulating these statistical uncertainties we use Poisson statistics. Experimental systematic errors, as long as they are related to measured properties of the detector, are expected to be dominantly Gaussian. We include flat theory errors based on the Rfit profile-likelihood construction [120, 121].

In part of our studies ratios of Higgs couplings will play a crucial role. Higher precision in measuring these ratios may naively be expected compared with individual measurements of couplings [62]. For such an improvement the analysis should not be statistics dominated, which it largely is however for an integrated luminosity of 30 fb^{-1}. Moreover, while experimental systematic uncertainties tend to cancel between the same Higgs decays but different production channels, the dominant theory errors are expected to cancel for identical production mechanisms. In line with these arguments we have found that using ratios does not significantly improve the results of Higgs sector analyses [63].

In this study we will show how κ as well as Γ_{hid} can be determined using SFitter. Starting from the completely exclusive likelihood map, SFitter determines the best-fitting point in the Higgs-sector parameter space. While a Bayesian probability analysis of the entire Higgs parameter space at the LHC is spoiled by noise, profile likelihoods can be studied in the vicinity of the best-fitting points [63]. In this analysis we assume that we already know the global structure of the likelihood map, so we can focus on the local properties around the SM-like solution. As it will turn out, alternative solutions can be studied nevertheless, for example with sign switches for some of the Higgs couplings.

Technically, the analysis presented in this thesis is based on the SFitter-Higgs setup. A list of all measurements and their different errors are shown in Tab. 4.1. Compared to previous analysis of the SFitter collaboration we have updated the numbers for the $H \to b\bar{b}$ channel in associated production with vector bosons from the recent ATLAS study [102], which confirms the previously obtained significances. The event rates for weak-boson-fusion production with decay into invisible states are adopted from Ref. [97]. The central data set is smeared around the theory predictions according to the theoretical error and the experimental errors, taking into account the correlations among the observables. For each

production	decay
ggH	ZZ
qqH	ZZ
ggH	WW
qqH	WW
WH	$WW(3l)$
WH	$WW(2l)$
$t\bar{t}H$	$WW(3l)$
$t\bar{t}H$	$WW(2l)$
inclusive	$\gamma\gamma$
qqH	$\gamma\gamma$
$t\bar{t}H$	$\gamma\gamma$
WH	$\gamma\gamma$
ZH	$\gamma\gamma$
qqH	$\tau\tau(2l)$
qqH	$\tau\tau(1l)$
$t\bar{t}H$	$b\bar{b}$
ZH	$b\bar{b}$
ZH	$llb\bar{b}$
ZH	$\nu\nu b\bar{b}$
qqH	ii

luminosity measurement	5 %
detector efficiency	2 %
lepton reconstruction efficiency	2 %
photon	4 %
WBF tag-jets	5 %
b-tagging efficiency	6 %
τ -tagging efficiency	3 %
lepton isolation efficiency ($H \to 4l$)	3 %
theory error	7 % / 14 %

Table 4.1.: On the left hand side, all channels that are taken into account for our analysis are shown. ggH denotes the gluon-fusion process, qqH is the vector-boson-fusion, $t\bar{t}H$ is the top-quark associated process, and ZH and WH are the Higgs-strahlung processes. The last channel (qqH) is the optional channel for additional invisible decays. On the right hand side, all errors considered in our work are shown. The theory error depends on the production process. For the gluon-fusion and the top-quark associated Higgs process, the error is 14% and for the other two processes 7%.

of the toy-experiments we determine the best-fit values. This numerical determination of the resulting parameter uncertainties is fitted to Gaussian distributions.

The new technical aspect of the present study is the more refined approach to the hypotheses tested: if we do not measure all Higgs couplings independently but instead test a given model hypothesis, the limits on the extracted model parameters improve significantly. Because this approach requires fewer measurements we now consider Higgs masses between 110 and 200 GeV and find a significant enhancement of the determination power for 30 fb^{-1} of LHC data at a collider energy of 14 TeV.

4.1. Higgs portal to hidden sector

The Standard Model, or extensions of it, may be connected to a hidden sector. An interesting realization of such a mechanism is provided by specifying the scalar Higgs domains in both sectors as the link between the two sectors [64–69]. To explore the possibility of detecting a hidden sector at the LHC we investigate a scenario in which the Standard Model Higgs sector is coupled to the hidden Higgs sector through quartic interactions. Such a scalar system is technically transparent and may therefore serve as paradigm for generic experimental features that could signal a hidden sector. There are many variants to this specific scenario, *e.g.* a hidden scalar sector without spontaneous symmetry breaking, large ensembles of scalar fields, etc. The scenarios can be disentangled by analyzing a few characteristic observables of the Higgs particles, in particular Higgs couplings. In this thesis we will concentrate on the simplest setup to quantify the potential of experimental analyses at the LHC.

The scenario we will focus on for now is described in Sec. 3.1. If the Higgs boson in the hidden sector acquires a vacuum expectation value then it leads to a mass mixing with the Standard Model Higgs boson. The mass eigenstates are a linear combination of the two Higgs bosons. The coefficients can be expressed by the mixing angle χ. It reads

$$\begin{aligned} h_1 = &\quad \cos\chi\, h_s + \sin\chi\, h_h \\ h_2 = &-\sin\chi\, h_s + \cos\chi\, h_h \,. \end{aligned} \tag{4.2}$$

Both, h_1 and h_2 couple to Standard Model fields through their h_s components and to the hidden sector through the h_h admixtures. To focus on generic features we assume the potential parameters λ_j and v_j to be of similar size and the mixing parameter η_χ to be moderate. The properties of h_1 then remain dominated by the Standard Model component, while the properties of h_2 are characterized primarily by the hidden Higgs component.

The phenomenology of a Higgs portal to the hidden sector depends on whether the standard Higgs particle is lighter or heavier than the new companion. In this study we assume that h_1 is light and mainly decays into Standard Model particles, at a rate reduced by mixing, and with an admixture of invisible decays to the hidden sector. The heavier h_2 bosons decay primarily into particles of the hidden sector, and only a small fraction by mixing to Standard Model particles and to light h_1 pairs. The production rate of h_2, mediated by mixing, is small. Since visible h_2 channels are suppressed by production and decay, we focus on the light Higgs boson h_1 closely related to the Standard Model.

All h_1 couplings to Standard Model particles are universally suppressed by the mixing parameter $\cos\chi$. In addition, h_1 may decay invisibly into the hidden sector. These two features imply

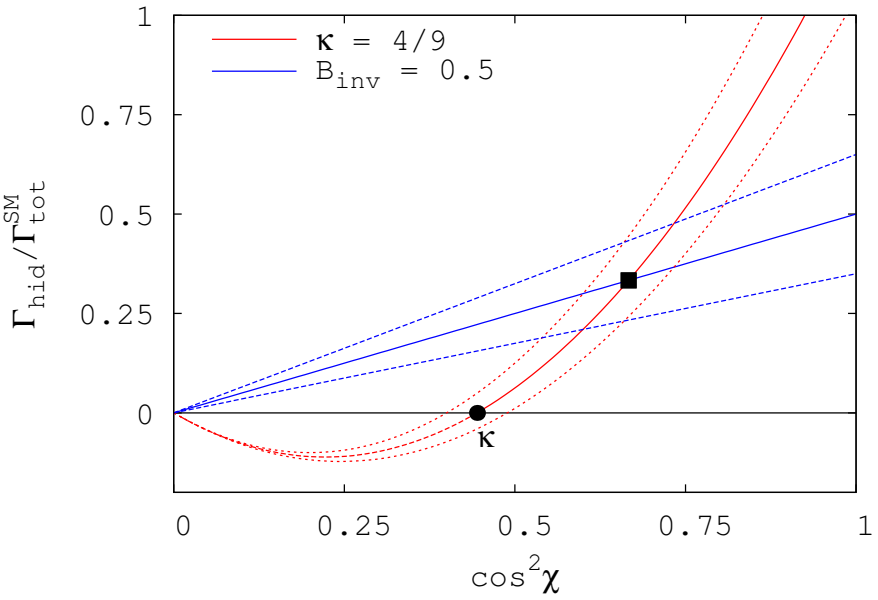

Figure 4.1.: Correlations between $\Gamma_{\rm hid}$ and $\cos^2\chi$ as defined in Eqs.(4.3), based on measuring κ and $\mathcal{B}_{\rm inv}$. The two parameters are set to $\kappa = 4/9$ and $\mathcal{B}_{\rm inv} = 0.5$, respectively, for illustration. The square marks the final solution of $\cos^2\chi = 2/3$ and $\Gamma_{\rm hid}/\Gamma^{\rm SM}_{\rm tot} = 1/3$ for this parameter set. The estimated 95% CL error bands are explained in the text.

$$\begin{aligned}\sigma &= \cos^2\chi\,\sigma^{\rm SM}\\ \Gamma_{\rm vis} &= \cos^2\chi\,\Gamma^{\rm SM}_{\rm vis}\\ \Gamma_{\rm inv} &= \cos^2\chi\,\Gamma^{\rm SM}_{\rm inv} + \Gamma_{\rm hid}\ .\end{aligned} \tag{4.3}$$

The two parameters $\cos\chi$ and $\Gamma_{\rm hid}$ will be determined in our LHC analysis. $\Gamma^{\rm SM}_{\rm inv}$ is generated by Higgs decays $H \to ZZ \to 4\nu$ with an invisible Z branching ratio of 4%. If invisible Higgs decays will be observed, this 4ν rate can be predicted from observed decays $H \to ZZ \to 4\ell$ and can thus be subtracted from the new-physics signal. For the sake of simplicity we will omit $\Gamma^{\rm SM}_{\rm inv}$ from now on.

If the invisible decay channel is open, the κ parameter in the twin ratio Eq. (4.1) reads in terms of the parameters $\cos\chi$ and $\mathrm{BR}_{\rm inv}$ (as generated by $\Gamma_{\rm hid}$):

$$\kappa = \frac{\cos^2\chi}{1+\mathcal{B}_{\rm inv}} \le 1 \quad \text{with} \quad \mathcal{B}_{\rm inv} = \frac{\mathrm{BR}_{\rm inv}}{\mathrm{BR}_{\rm vis}} = \frac{\mathrm{BR}_{\rm inv}}{1-\mathrm{BR}_{\rm inv}}\,. \tag{4.4}$$

$\mathcal{B}_{\rm inv}$ can also be expressed as the ratio of invisible decays to just one visible decay channel d, $\mathcal{B}_{\rm inv} = {\rm BR}_{\rm inv}/({\rm BR}_d/{\rm BR}_d^{\rm SM})$. It can thus be observed without explicit reference to the total width. For $\sin\chi \ll 1$ $\mathcal{B}_{\rm inv}$ simply approaches ${\rm BR}_{\rm inv}$.

For the Higgs portal the parameters κ and $\mathcal{B}_{\rm inv}$ are independent of the analysis channels. As a result, ratios of visible branching ratios are not modified ${\rm BR}_{d_1}/{\rm BR}_{d_2} = ({\rm BR}_{d_1}/{\rm BR}_{d_2})^{\rm SM}$. The observation of these identities provides a necessary consistency test for the hidden Higgs scenario.

The detailed experimental analysis of such a scenario will proceed in two steps: As long as only κ is measured but invisible Higgs decays are not, upper bounds on the mixing and, in parallel, on the fraction of invisible h_1 decays can be established,

$$\sin^2\chi \leq 1-\kappa \quad \text{and} \quad {\rm BR}_{\rm inv} \leq 1-\kappa\,, \tag{4.5}$$

constraining the potential impact of the hidden sector on the properties of the SM-type Higgs boson. With κ measured, the hidden h_1 partial width will be correlated with the mixing parameter

$$\frac{\Gamma_{\rm hid}}{\Gamma_{tot}^{\rm SM}} = \cos^2\chi\left(\frac{\cos^2\chi}{\kappa}-1\right)\,, \tag{4.6}$$

as illustrated in Fig. 4.1 for $\kappa = 4/9$. For illustration purposes, the error on κ in this figure is chosen to be 10%.

Even though $\mathcal{B}_{\rm inv}$ can be in principle be determined experimentally, precise measurements of the invisible decay mode are difficult at the LHC. To show the correlation of the two parameters with the two observables we choose $\mathcal{B}_{\rm inv} = 0.5$ with a relative error of 30%, as expected for the final integrated luminosity of 300 fb^{-1} [95–99]. Combining Eq. (4.6) with the definition Eq. (4.4),

$$\frac{\Gamma_{\rm hid}}{\Gamma_{tot}^{\rm SM}} = \cos^2\chi\,\mathcal{B}_{\rm inv}\,, \tag{4.7}$$

allows us to determine both the mixing parameter $\cos\chi$ and the h_1 partial width to the hidden sector $\Gamma_{\rm hid}$ individually, *cf.* Fig. 4.1:

$$\cos^2\chi \;=\; \frac{\kappa}{1-{\rm BR}_{\rm inv}} \qquad \text{and} \qquad \frac{\Gamma_{\rm hid}}{\Gamma_{tot}^{\rm SM}} = \frac{\kappa\,{\rm BR}_{\rm inv}}{(1-{\rm BR}_{\rm inv})^2}\,. \tag{4.8}$$

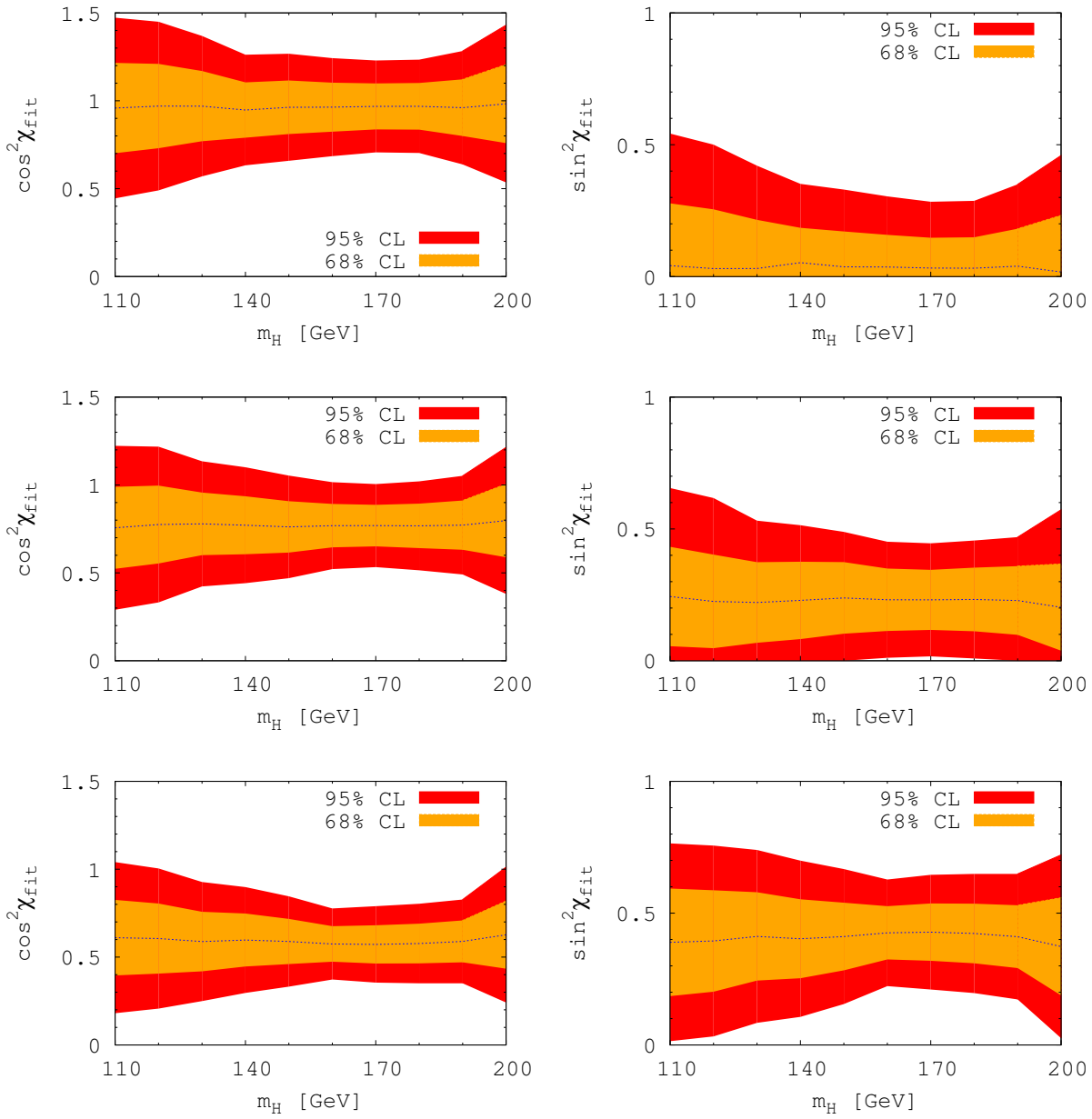

Figure 4.2.: LHC sensitivity to modified Higgs couplings and no invisible decays $\Gamma_{\text{hid}} = 0$, based on 30 fb^{-1} of data. Left: measurement errors as a function of the Higgs mass for $\cos^2\chi_{\text{th}} = 1.0$ (top), $\cos^2\chi_{\text{th}} = 0.8$ (center) and $\cos^2\chi_{\text{th}} = 0.6$ (bottom). Right: resulting upper and lower bounds on the mixing parameter $\sin^2\chi$, constrained to the physical range.

m_H	$\cos\chi$	68% CL	95% CL
110	0.96	0.26	0.52
120	0.97	0.24	0.48
130	0.97	0.20	0.40
140	0.95	0.16	0.32
150	0.96	0.15	0.30
160	0.96	0.14	0.28
170	0.97	0.13	0.26
180	0.97	0.13	0.26
190	0.96	0.16	0.26
200	0.98	0.22	0.32

Table 4.2.: For the Standard Model hypothesis, the fitted results for $\cos\chi$ together with the 68% and 95% confidence level (CL), in this case the one and two standard deviations, are shown for various Higgs masses with an integrated luminosity of 30 fb^{-1}.

The bands around the intersection point and their projections on the axes indicate the 95% CL for the parameters $\cos^2\chi$ and Γ_{hid}.

In a Higgs sector likelihood analysis we can ask three kinds of questions:

1. Can we determine a non-zero mixing $\kappa \neq 1$ from a sizable Higgs sample at all?

2. To shut a Higgs portal, what size of κ can we exclude if we observe Standard Model couplings within given experimental and theory errors?

3. To verify the Higgs portal, which finite values of κ can we establish as a deviation from the Standard Model within errors. How do invisible Higgs decays affect this measurement?

To answer the first questions, the upper panels in Fig. 4.2 show the bounds on $\kappa = \cos^2\chi$ which we can set by analyzing a sample of Standard Model Higgs bosons with masses

M_H [GeV]	$\kappa >$		$\sin^2\chi, \text{BR}_{\text{inv}} <$		$\Gamma_{\text{hid}}/\Gamma^{\text{SM}}_{\text{tot}} <$	
120	0.50	0.76	0.50	0.24	1.0	0.32
160	0.70	0.82	0.30	0.18	0.43	0.22
200	0.54	0.73	0.46	0.27	0.85	0.37

Table 4.3.: Upper bounds (95% CL) on mixing and invisible decays expected to be set in a Higgs sample within the Standard Model for integrated luminosities of 30 (left) and 300 fb^{-1} (right).

between 110 and 200 GeV. We neglect invisible Higgs decays in this first step, but all standard Higgs search channels are exploited based on an integrated luminosity of 30 fb^{-1} [63]. Starting with the Standard Model hypothesis at $m_H = 120$ GeV we can measure $\cos^2\chi = 1 \pm 24\%(48\%)$ at the 68%(95%) CL. The results for the other Higgs masses are shown in Tab. 4.1. For larger Higgs masses the error bar improves by a factor of two, due to an increased statistics of the comparably clean WW and ZZ channels. For even larger Higgs masses around 200 GeV the over-all event rate drops again, increasing the measurement error again. As shown in the lower panels of Fig. 4.2 we can also translate the minimal values of κ into maximal values of the mixing parameter $\sin^2\chi$ according to Eq. (4.5). In contrast to the upper limits on $\cos^2\chi$ the limits on $\sin^2\chi$ include the constraint $0 \leq \sin^2\chi \leq 1$. In Tab. 4.3 we collect the bounds on a modified Higgs coupling, including the constraint, for three Higgs masses, based on an integrated luminosity of 30 fb^{-1} as well as expectations for an integrated luminosity of 300 fb^{-1}. Even without observing invisible decays explicitly, we can translate these results into upper bounds on the invisible decay width according to Eq. (4.4). These bounds are shown in the right column of the table.

The error on the scaled Higgs couplings includes another square root, which translates into a relative error $(\Delta g)/g \sim 10\%(20\%)$. These limits measure how well the Higgs mechanism in the Standard Model can be established quantitatively, and they have to be compared to an independent variation of all Higgs couplings, which for $m_H = 120$ GeV are expected to be measured to $\mathcal{O}(25\%-50\%)$ [63]. The sizable improvement of the constrained analysis arises first of all because all experimental channels now contribute to the same measurement, and secondly because they also determine the total Higgs width much more precisely than the $H \to b\bar{b}$ fat-jet analysis.

Before moving away from Standard Model decays only, we show the results of a two-parameter fit in the upper panels of Fig. 4.3, while keeping $\Gamma_{hid} = 0$. Compared to the one-dimensional parameter extraction shown in Fig. 4.2 the error on the extracted value of $\cos^2\chi$ is now increased. This arises because we now have to perform a two-dimensional parameter extraction and project the correlated uncertainty onto the two model parameters $\cos\chi$ and Γ_{hid}. Comparing the upper panels of Fig. 4.3 to Fig. 4.2 shows this effect on the extracted parameters, just fitting two parameters without even introducing an invisible Higgs decay. The error on $\cos^2\chi$ becomes asymmetric due to the positivity constraint on the Higgs width, fixing the upper error band of $\cos^2\chi$. On the other hand, fake invisible-decay events from background fluctuations lead to a wide lower error bound. Moreover, we observe a clear bias towards too large event numbers towards small values of $\cos^2\chi$. This is in part due to the asymmetric Poisson distribution and in part due to the fact that measurement channels where the number of background events from the control region exceeds the number of events in the signal region, are explicitly excluded from the fit. A more detailed discussion of this effect is presented in App. E. Finally, the error band for the extracted Γ_{hid} ranges around 20% of the Standard Model width.

The impact of actual invisible decays is estimated by choosing $\Gamma_{\text{hid}} = \sin^2\chi\,\Gamma_{\text{tot}}^{\text{SM}}$ as illustrative example for the parametrization of the non-zero invisible partial width. This

parametrization accounts naturally for the suppression of Γ_{hid} by mixing, while a coefficient of size $\Gamma_{\text{tot}}^{\text{SM}}$ would be expected for structures in the hidden sector roughly parallel to the standard sector [64–67]. Comparing the top left and top right panels of Figure 4.3, it is evident that the effect of an actual invisible Higgs decay on the extraction of $\cos^2\chi$ is small. A measurement of the invisible Higgs width, beyond setting upper bounds, seems challenging with only 30 fb^{-1} of integrated luminosity. The best discrimination power we obtain for medium-sized values of $\cos^2\chi$, where we have a significant invisible branching ratio and the production side is not strongly suppressed.

Finally, in the right panels we see a clear correlation between the two extracted parameters, owed to the form of the observables shown in Eq. (4.4) and Fig. 4.1.

4.2. Strongly-interacting Higgs boson

Deviations of the Higgs couplings similar to the $\cos\chi$ factor in Eq. (4.3) are expected when a light Higgs boson is generated as a pseudo-Goldstone boson by global symmetry breaking in a new strong interaction sector. Depending on the details of the model, the Higgs couplings are modified either individually for different particle species, or universally for all species [75–79]. In contrast to the hidden Higgs model, the light Higgs boson h_1 does not decay into channels not present in the Standard Model.

Such a picture can be developed using Holographic Higgs Models, based on the AdS/CFT correspondence, in which strongly coupled theories in four dimensions are identified with weakly coupled theories in five dimensions [122–126]. For example, the spontaneous breaking of a global symmetry $SO(5) \to SO(4)$ generates the adequate iso-doublet of Goldstone bosons. Assigning the Standard Model fermions either to spinorial or fundamental $SO(5)$ representations changes the Higgs couplings either universally or separately for Standard Model vectors and fermions. The modifications are determined by the parameter

$$\xi = \left(\frac{v}{f}\right)^2 \tag{4.9}$$

which measures the magnitude of the Goldstone scale f in relation to the standard Higgs vacuum expectation value v. The case where all Higgs couplings are suppressed universally by a factor $(1-\xi)^{1/2}$, is covered by the analysis in the preceding section identifying

$$\kappa \equiv 1 - \xi\,. \tag{4.10}$$

All results from the Higgs portal can be transferred one-by-one to this universal strong interaction model, identifying $\cos^2\chi \to 1-\xi$ and setting $\mathcal{B}_{\rm inv}=0$. Hence, it can be concluded from Fig. 4.2 that ξ can be measured with an uncertainty of $10\%-20\%$, depending on the Higgs mass.

In a closely related scenario [79] universality is broken to the extent that the Higgs coupling of vector particles is reduced, still, by $(1-\xi)^{1/2}\approx 1-\xi/2$ but the coupling of fermions by a different coefficient, $(1-2\xi)/(1-\xi)^{1/2}\approx 1-3\xi/2$. Now, the two κ parameters of the twin width-ratios, at small ξ, read

$$\begin{aligned}\kappa_V &= 1-\left[1(3)-2\,\text{BR}_\text{f}^\text{SM}\right]\,\xi \\ \kappa_f &= 1-\left[3(5)-2\,\text{BR}_\text{f}^\text{SM}\right]\,\xi\,,\end{aligned} \tag{4.11}$$

The indices V, f distinguish vector and fermion Higgs decays, and the expression in brackets corresponds to production either in Higgs-strahlung/electroweak boson fusion or — altered to () — in gluon fusion; $\text{BR}_\text{f}^\text{SM}$ denotes the inclusive Higgs branching ratio to fermions in the Standard Model which is close to one for light Higgs bosons.

The two κ parameters of this non-universal strong interaction model are characteristically different from both the universal strong interaction model as well as the Higgs portal. First, they are different for vector and fermion decays of the Higgs particle; second, in parameter regions in which more than half of the Higgs decays are fermionic, κ_V is larger than unity for Higgs-strahlung/electroweak fusion.

Results for this model are presented in Fig. 4.4 and in Tab. 4.4 for 30 and 300 fb^{-1}. At low luminosity two solutions emerge, while an increased luminosity eliminates the fake solution in major parts of the parameter space, as long as the Higgs mass is small. The mathematical evolution of the two solutions and their analytical form is discussed in App. F. Around $\xi\sim 0.5$ the observable rates at the LHC drop sharply, not allowing for a reliable extraction of ξ simply based on too little statistics for the fit. Therefore, the Gray bands blind ranges of parameter space in which the modified theory leads to too large a suppression. Only when our fit finds $\chi^2/\text{d.o.f.}\gtrsim 1$ (d.o.f. denotes degrees of freedom) the result becomes statistically trustworthy again.

In contrast to 120 GeV, we observe that the situation hardly improves for a 200 GeV Higgs boson once we go to higher luminosity. For this mass only four Higgs channels are left. All include a decay into either W or Z bosons, and on the production side three of them are proportional to g_{ttH}, either via gluon-fusion or top-quark associated production. These three measurements are equivalent and exhibit an ambiguity because fermion-Higgs couplings cannot distinguish between small and large values of ξ, see App. F. Only the fourth measurement based on weak-boson fusion production can resolve the ambiguity.

		30 fb^{-1}					
M_H [GeV]	ξ_{th}	ξ_1	$\Delta\xi_1$	w_{ξ_1}	ξ_2	$\Delta\xi_2$	w_{ξ_2}
120	0.0	-0.04	0.36	0.94	0.67	0.06	0.06
	0.2	0.16	0.26	0.88	0.63	0.06	0.12
	0.6	0.61	0.06	0.54	0.26	0.18	0.46
160	0.0	0.0	0.12	0.98	0.73	0.03	0.02
	0.2	0.20	0.10	0.95	0.69	0.04	0.05
	0.6	0.64	0.06	0.85	0.33	0.10	0.15
200	0.0	0.01	0.16	0.84	0.77	0.03	0.16
	0.2	0.19	0.14	0.67	0.71	0.04	0.33
	0.6	0.67	0.06	0.50	0.30	0.16	0.50
		300 fb^{-1}					
M_H [GeV]	ξ_{th}	ξ_1	$\Delta\xi_1$	w_{ξ_1}	ξ_2	$\Delta\xi_2$	w_{ξ_2}
120	0.0	0.0	0.14	0.99	0.67	0.08	0.01
	0.2	0.20	0.08	0.99	0.63	0.02	0.01
	0.6	0.60	0.02	0.96	0.31	0.04	0.04
160	0.0	0.0	0.08	1.0	—	—	0
	0.2	0.20	0.08	0.99	0.67	0.04	0.01
	0.6	0.63	0.04	0.96	0.36	0.08	0.04
200	0.0	0.0	0.10	0.92	0.75	0.014	0.08
	0.2	0.19	0.10	0.79	0.69	0.018	0.21
	0.6	0.63	0.03	0.55	0.31	0.16	0.45

Table 4.4.: Errors $\Delta\xi$ (95% CL) on the pseudo-Goldstone parameter ξ for integrated luminosities of 30 (top) and 300 fb^{-1} (botoom). Shown are the two solutions together with their corresponding probability w_ξ of the best-fit, which are the relative numbers of toy experiments ending up in the vicinity (as obtained by a fit of two Gauss peaks) of this solution.

Even though this channel is comparably clean, it is systematics limited, *i.e.* it hardly improves with higher luminosities.

The two solutions shown in Fig. 4.4 also represent a technical challenge. We need to know not only the error $\Delta\xi$ on the individual solution, but also the probability w_ξ with which this solution appears. A Minuit fit per toy-experiment alone cannot achieve this, because there is no guarantee that it will find the global minimum of χ^2. Indeed, we observe a strong dependence on the starting point in Minuit. Therefore, we need to add a coarse grid scan of the one-dimensional parameter space before the minimization. To obtain the 68% and 95% confidence levels in Fig. 4.4 we first fit a sum of two Gaussians to the parameter distribution. To extract a confidence level interval around each of the two peaks we define a height which crosses both Gaussians such that the sum of the two central areas corresponds to 68% or 95% of the entire integral under both Gaussians. The two intersections of this

horizontal line with each Gaussian give us the confidence regions quoted for example in Fig. 4.4.

First of all, in Fig. 4.4 we again see that the typical error bars shrink when we increase the Higgs mass and with it the number of events from 120 GeV to 160 GeV. For even larger Higgs masses some of the relevant channels rapidly vanish, so the error bars increase again. The actual error bars for the different scenarios are listed in Tab. 4.4. In particular for moderate luminosity the absolute error on ξ_1, for assumed values of $\xi_{\text{th}} < 0.2$ range around 20% for a light Higgs boson and well below 10% towards larger mass. These numbers again roughly compare to the typical values for $\Delta\xi$ in the universal strongly interacting model or $\sqrt{\Delta\kappa}$ for the Higgs portal. For larger values of $\xi \geq 0.6$ the two strongly interacting models start deviating significantly. In particular, the relative error $\Delta\xi_1/\xi_1$ decreases dramatically. The reason will be discussed in detail in App. F: due to the non-universal structure of the fermion and vector couplings in this range the Higgs event rates vary much more strongly than elsewhere. Therefore, the LHC will probe this region with high precision, with the slight caveat that towards slightly smaller ξ the Higgs production and decay rates vanish rapidly. These are precisely the dangerous Gray regions in Fig. 4.4 — as long as we observe Higgs events at the LHC the sharp drop in rates towards $\xi = 0.5$ is a welcome feature to analyze the model at colliders.

The improvement of the errors with increased statistics is also shown in Tab. 4.4. If the measurement were statistics dominated, the error would be reduced by a factor $\sqrt{10} \simeq 3$ when going from 30 to 300 fb^{-1}. From the results we find that the improvement is smaller. The reason is that all measurements determine only a single parameter, so unlike in the unconstrained Higgs sector analysis [63] in the current setup even for 30 fb^{-1} the results are not entirely statistics dominated.

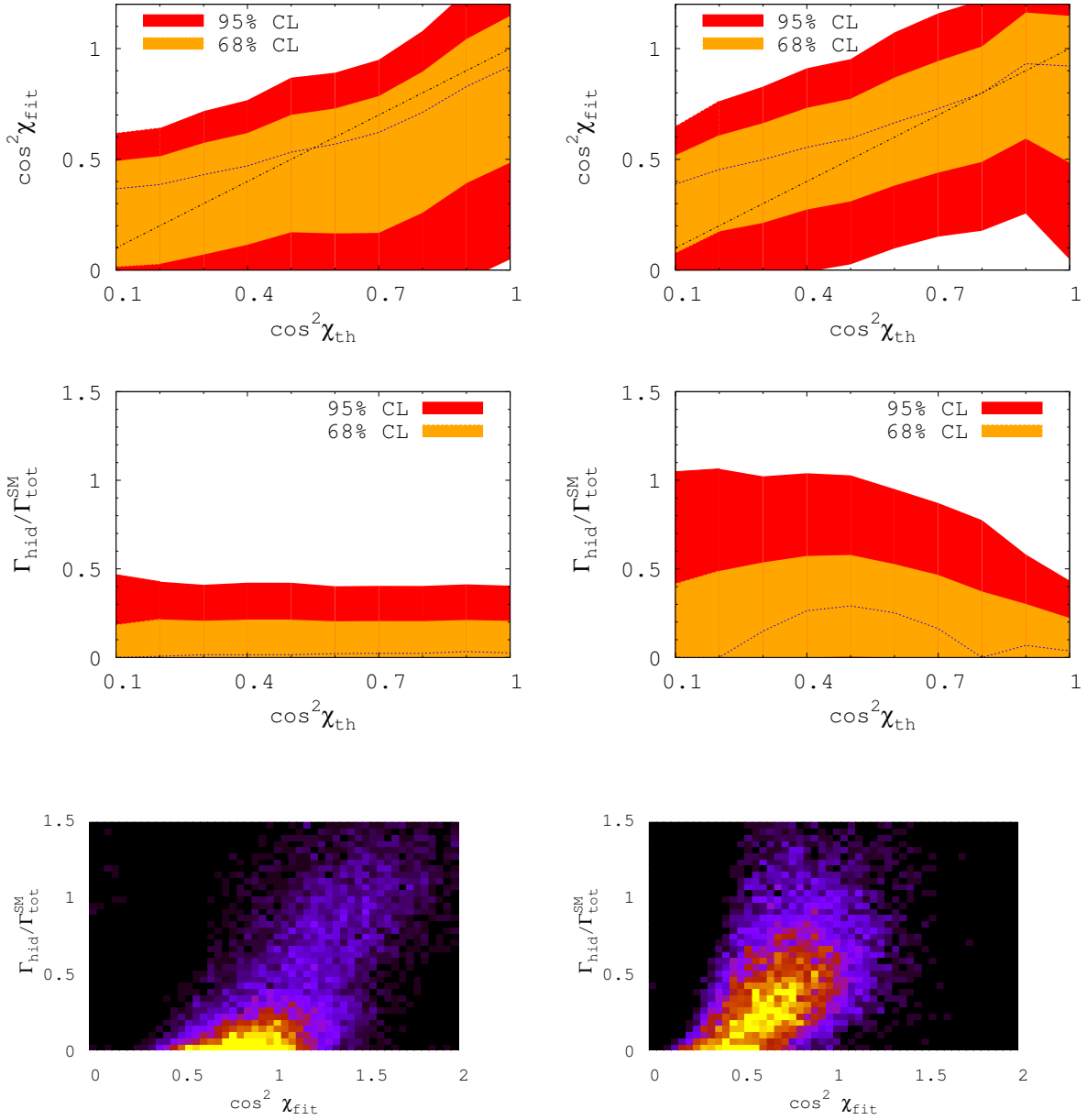

Figure 4.3.: LHC sensitivity to modified Higgs couplings and invisible decays, based on 30 fb^{-1} of data. Left column: $\Gamma_{\text{hid}} = 0$; right column $\Gamma_{\text{hid}} = \sin^2\chi\,\Gamma^{\text{SM}}_{\text{tot}}$ for invisible decays. The Higgs mass is fixed to 120 GeV. Top row: extracted $\cos^2\chi_{\text{fit}}$ values as a function of $\cos^2\chi_{\text{th}}$; Center row: extracted bounds and measurements of $\Gamma_{\text{hid}}/\Gamma^{\text{SM}}_{\text{tot}}$ as a function of $\cos^2\chi_{\text{th}}$; Bottom row: illustration of the correlation between mixing and invisible partial width using $\cos^2\chi_{\text{th}} = 1.0$ (left column) and 0.6 (right column).

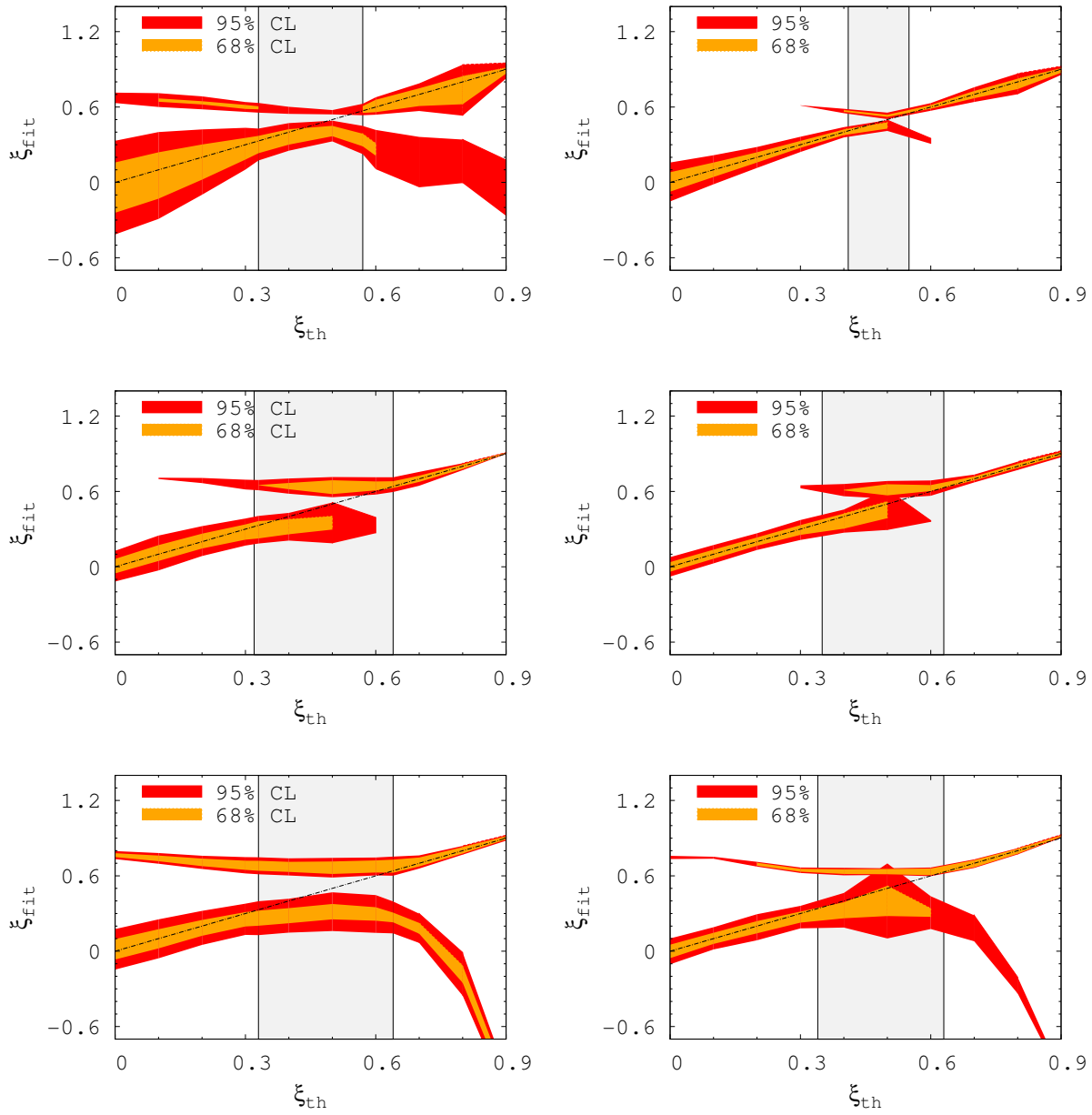

Figure 4.4.: LHC sensitivity to modified Higgs couplings based on 30 (left column) and 300 fb^{-1} (right column) for un-aligned boson and fermion couplings as a function of the assumed ξ_{th} for $m_H = 120$ GeV (top), 160 GeV (center) and 200 GeV (bottom). ξ values close to 1/2, for which the rates are strongly suppressed, are blinded by the gray bars.

5. Summary and discussion

In this thesis we have analyzed the LHC reach for deviations of Higgs couplings from their Standard Model values. Two models can be linked to such signatures: First, we couple the Standard Model Higgs field to a hidden Higgs sector, opening a renormalizable Higgs portal between the two sectors. From the event rates for visible Higgs production and decay channels we could derive upper bounds on non-SM admixtures in the wave-function of the Higgs boson and on novel invisible decay channels. Since it is unclear if at the LHC we will be able to quantitatively analyze invisible Higgs decays, given the experimental errors, the question arises if we include the invisible Higgs decay rate in a two-dimensional fit or only include modified visible couplings.

From the two-dimensional fit we find 95% CL limits on the two model parameters $\sin^2\chi < 0.50$ and $\Gamma_{\text{hid}}/\Gamma_{\text{tot}}^{\text{SM}} < 1.0$ ($\mathcal{L} = 30$ fb^{-1} and $m_H = 120$ GeV). Towards Higgs masses around 160 GeV these limits slightly improve, while for even heavier masses the decreasing production rates at the LHC take their toll. These numbers correspond to a 10% to 20% measurement of the modified Higgs couplings $(\Delta g)/g$. Such bounds also quantify to what accuracy a Higgs boson discovered and studied at the LHC could be identified as the Standard Model realization. They should be compared to limits on the individual Higgs couplings from general Higgs sector analyses [62, 63] and they show a significant improvement driven by the higher level of specification in the hypothesis tested.

Neglecting the invisible Higgs decay and hence trading the minimal amount of extra information for the advantage of a one-dimensional fit without additional noise in a small region of parameter space ($m_H \sim 160$ GeV and $\cos^2\chi \sim 0.6$) we might even be able to establish a Higgs portal at the 5σ level based on an integrated luminosity of 30 fb^{-1}.

If invisible decay channels of the Higgs boson are indeed measured, the mixing parameter and the partial width for Higgs decays to the hidden sector can of course be determined individually. However, such a measurement will likely require higher luminosities.

A related problem arises when a light Higgs boson is identified with a pseudo-Goldstone boson associated with the spontaneous breaking of global symmetries in new strong interactions. If fermion and vector couplings are scaled equally, the scaling analysis of the hidden sector can be transcribed without change, assuming there are no Higgs decays into non-SM channels. The bound on $\sin^2\chi$ can simply be read as a bound on ξ.

More interestingly, if the Higgs couplings are modified separately for vectors and fermions, various production/decay channels may be analyzed individually so that a unique picture emerges. For small values of ξ the two kinds of couplings at least qualitatively scale similarly, so our results for $(\Delta\xi)/\xi$ follow the usual patterns. For larger values around $\xi \sim 0.5$ the Higgs-fermion couplings now vanish, leading to wells in the Higgs event rates. In those regions the relative error on the determination of ξ can shrink to 5%, though being dangerously close to parameter regions where the Higgs discovery would require larger LHC luminosities.

The LHC will be able to probe scenarios with modified Higgs couplings as generally analyzed in Refs. [62, 63]. However, testing a specific one- or two-parameter model appears to be a promising strategy to gain insight into the Higgs sector already based on an integrated luminosity of 30 fb^{-1} at 14 TeV. Compared to the general analysis the typical error bars on Higgs couplings are reduced by at least a factor 1/2, now ranging around 10% to 20% for Higgs masses between 120 GeV and 200 GeV.

A. Passarino-Veltman reduction

In loop calculations involving fermions in the loop tensor integrals appear. Tensor integrals have powers of the loop momentum in the nominator. Passarino and Veltman [44] found a technique to get rid of these integrals and reduce them to scalar n-point functions. The advantage of this reduction is that we only have to know some master integrals. The Passarino-Veltman reduction method can be used in computer calculation, e.ġ., FEYNCALC [45]. In this appendix, we want to show how the reduction works for two- and three-point functions up to rank two tensors. A tensor integral in the most general form that has N propagators in the loop reads

$$T^N_{\mu_1\dots\mu_M}(p_1,\dots,p_{N-1},m_0,\dots,m_{N-1}) = \int \frac{d^4q}{i\pi^2}\frac{q_{\mu_1}\dots q_{\mu_M}}{D_0\dots D_{N-1}}\,. \tag{A.1}$$

The propagators in the denominator and the external momenta are defined by

$$D_i = (q+p_i)^2 - m_i^2, \quad p_i = \sum_{j=0}^{i} p'_j, \quad p_0 = 0, \quad i \in \{0,\dots,N-1\}\,. \tag{A.2}$$

The following two abbreviations are useful for the calculation

$$f_i = p_i^2 - m_i^2 + m_0^2, \quad p_{ij} = p_i - p_j\,. \tag{A.3}$$

With the definition in (A.2) follows

$$p_i \cdot q = \frac{1}{2}\left(D_i - D_0 - f_i\right)\,. \tag{A.4}$$

These relations will be used many times in the reduction. The loop momenta will be integrated out, but the tensor structure remains. There are only the external momenta and the metric that can keep the tensor structure. Thus, we can expand the two- and three-point tensor function in the external momenta which is given by

$$\begin{aligned} B^{\mu} &= p_1^{\mu} B_1 \\ B^{\mu\nu} &= p_1^{\mu} p_1^{\nu} B_{11} + \eta^{\mu\nu} B_{00} \\ C^{\mu} &= p_1^{\mu} C_1 + p_2^{\mu} C_2 \\ C^{\mu\nu} &= p_1^{\mu} p_1^{\nu} C_{11} + \left(p_1^{\mu} p_2^{\nu} + p_2^{\mu} p_1^{\nu}\right) C_{12} + p_2^{\mu} p_2^{\nu} C_{22} + \eta^{\mu\nu} C_{00} \,. \end{aligned} \tag{A.5}$$

On the right hand side of the equations above, new functions are introduced. The next task is to calculate them.

A.1. Reduction of a two-point tensor integral of rank one

Starting with the easiest case, we only need to determine one function B_1 that means one equation is enough. Contracting the first line of Eq. (A.5) with $p_{1\mu}$ and using Eq. (A.4) yields

$$\begin{aligned} p_1^2 B_1 = p_{1\mu} B^{\mu} &= \int \frac{d^4q}{i\pi^2} \frac{p_1 \cdot q}{D_0 D_1} \\ &= \int \frac{d^4q}{i\pi^2} \frac{1}{2} \left(\frac{1}{D_0} - \frac{1}{D_1} - \frac{f_1}{D_0 D_1} \right) \\ &= \frac{1}{2} \left(A_0(m_0) - A_0(m_1) - f_1 B_0(p_1, m_0, m_1) \right) \,, \end{aligned} \tag{A.6}$$

and the final result is

$$B_1(p_1, m_0, m_1) = \frac{1}{2p_1^2} \left(A_0(m_0) - A_0(m_1) - f_1 B_0(p_1, m_0, m_1) \right) \,. \tag{A.7}$$

The tensor integral B^{μ} is determined by the one- and two-point scalar functions.

A.2. Reduction of a two-point tensor integral of rank two

Analogously to the previous section, we have to determine two functions. Thus, we need at least two independent equations. Contracting $B^{\mu\nu}$ in the second line of Eq. (A.5) with $p_{1\mu}$ and the metric tensor, it follows

$$\begin{aligned} p_{1\mu} B^{\mu\nu} =& p_1^\nu \left(B_{00} + p_1^2 B_{11} \right) \\ \eta_{\mu\nu} B^{\mu\nu} =& 4B_{00} + p_1^2 B_{11} \,. \end{aligned} \tag{A.8}$$

For the left hand side, we get

$$\begin{aligned} p_{1\mu} B^{\mu\nu} &= \int \frac{d^4q}{i\pi^2} \frac{p_1 \cdot q q^\nu}{D_0 D_1} \\ &= \int \frac{d^4q}{i\pi^2} \frac{1}{2} \left(\frac{q^\nu}{D_0} - \frac{q^\nu}{D_1} - f_1 \frac{q^\nu}{D_0 D_1} \right) \\ &= \frac{1}{2} p_1^\nu \left(A_0(m_1) - f_1 B_1(p_1^2, m_0, m_1) \right) \,. \end{aligned} \tag{A.9}$$

The first integral in the second line vanishes because the nominator is odd and the denominator of the integrand is even. For the second integral, I used the substitution $q \to q + p_1$. The result for the second equation is

$$\begin{aligned} \eta_{\mu\nu} B^{\mu\nu} &= \int \frac{d^4q}{i\pi^2} \frac{q^2}{D_0 D_1} \\ &= A_0(m_1) + m_0^2 B_0(p_1, m_0, m_1) \,. \end{aligned} \tag{A.10}$$

We can put the equations together, cancel p^ν in the first equation, and get a system of linear equations

$$\begin{aligned} B_{00} + p_1^2 B_{11} =& \frac{1}{2} \left(A_0(m_1) - f_1 B_1(p_1, m_0, m_1) \right) \\ 4B_{00} + p_1^2 B_{11} =& A_0(m_1) + m_0^2 B_0(p_1, m_0, m_1) \,, \end{aligned} \tag{A.11}$$

with the final result

$$\begin{aligned} B_{00} =& \frac{1}{6} \left(A_0(m_1) + 2m_0^2 B_0(p_1^2, m_0, m_1) + f_1 B_1(p_1, m_0, m_1) \right) \\ B_{11} =& \frac{1}{3p_1^2} \left(A_0(m_1) - 2f_1 B_1(p_1, m_0, m_1) - m_0^2 B_0(p_1, m_0, m_1) \right) \,. \end{aligned} \tag{A.12}$$

As we have seen before, B_1 is determined by one- and two-point scalar function.

A.3. Reduction of a three-point tensor integral of rank one

Contracting the third line of Eq. (A.5) n with $p_{1\mu}$ and $p_{2\mu}$ gives

$$\begin{aligned} p_{1\mu}C^{\mu} &= p_1^2 C_1 + p_1 \cdot p_2 C_2 \\ p_{2\mu}C^{\mu} &= p_1 \cdot p_2 C_1 + p_2^2 C_2 \,. \end{aligned} \tag{A.13}$$

For the left hand side follows for the first equation

$$\begin{aligned} p_{1\mu}C^{\mu} &= \int \frac{d^4q}{i\pi^2} \frac{p_1 \cdot q}{D_0 D_1 D_2} \\ &= \int \frac{d^4q}{i\pi^2} \frac{1}{2} \left(\frac{1}{D_0 D_2} - \frac{1}{D_1 D_2} - f_1 \frac{1}{D_0 D_1 D_2} \right) \\ &= \frac{1}{2} \left(B_0(p_2, m_0, m_2) - B_0(p_2 - p_1, m_1, m_2) - f_1 C_0(p_1, p_2, m_0, m_1, m_2) \right) \,, \end{aligned} \tag{A.14}$$

and for the second equation

$$p_{2\mu}C^{\mu} = \frac{1}{2} \left(B_0(p_1, m_0, m_2) - B_0(p_2 - p_1, m_1, m_2) - f_2 C_0(p_1, p_2, m_0, m_1, m_2) \right) \,. \tag{A.15}$$

This yields the system of linear equations

$$\begin{aligned} p_1^2 C_1 + p_1 \cdot p_2 C_2 =& \frac{1}{2} \left(B_0(p_2, m_0, m_2) - B_0(p_{21}, m_1, m_2) - f_1 C_0(p_1, p_2, m_0, m_1, m_2) \right) \\ p_1 \cdot p_2 C_1 + p_2^2 C_2 =& \frac{1}{2} \left(B_0(p_1, m_0, m_2) - B_0(p_{21}, m_1, m_2) - f_2 C_0(p_1, p_2, m_0, m_1, m_2) \right) \,. \end{aligned} \tag{A.16}$$

In the case

$$p_1^2 = 0, \quad p_1 \cdot p_2 = \frac{m_H^2}{2}, \quad p_2^2 = m_H^2 \tag{A.17}$$

the result is

$$\begin{aligned} C_1 =& \frac{1}{m_H^2}\left(B_0(p_1,m_0,m_2) - B_0(p_2,m_0,m_2) - (f_2-f_1)C_0(p_1,p_2,m_0,m_1,m_2)\right) \\ C_2 =& \frac{1}{m_H^2}\left(B_0(p_2,m_0,m_2) - B_0(p_{21},m_1,m_2) - f_1 C_0(p_1,p_2,m_0,m_1,m_2)\right) . \end{aligned} \tag{A.18}$$

A.4. Reduction of a three-point tensor integral of rank two

Contracting the fourth line of Eq. (A.5) with $p_{1\mu}$, $p_{2\mu}$ and the metric tensor yields the right hand sides

$$\begin{aligned} p_{1\mu}C^{\mu\nu} &= p_1^\nu C_{00} + p_1^\nu p_1^2 C_{11} + \left(p_2^\nu p_1^2 + p_1^\nu p_1\cdot p_2\right) C_{12} + p_2^\nu p_1\cdot p_2 C_{22} \\ p_{2\mu}C^{\mu\nu} &= p_2^\nu C_{00} + p_1^\nu p_1\cdot p_2 C_{11} + \left(p_1^\nu p_2^2 + p_2^\nu p_1\cdot p_2\right) C_{12} + p_2^\nu p_2^2 C_{22} \\ \eta_{\mu\nu}C^{\mu\nu} &= 4C_{00} + p_1^2 C_{11} + 2p_1\cdot p_2 C_{12} + p_2^2 C_{22} , \end{aligned} \tag{A.19}$$

and the left hand side of the first

$$\begin{aligned} p_{1\mu}C^{\mu\nu} =& \int \frac{d^4q}{i\pi^2}\frac{1}{2}\left(\frac{q^\nu}{D_0D_2} - \frac{q^\nu}{D_1D_2} - f_1\frac{q^\nu}{D_0D_1D_2}\right) \\ =& \frac{1}{2}\left(p_2^\nu B_1(p_2,m_0,m_2) + p_{21}^\nu B_1(p_{21},m_1,m_2) + p_1^\nu B_0(p_{21},m_1,m_2)\right. \\ & \left. -\frac{1}{2}p_1^\nu f_1 C_1 - \frac{1}{2}p_2^\nu f_1 C_2\right) , \end{aligned} \tag{A.20}$$

second

$$\begin{aligned} p_{2\mu}C^{\mu\nu} =& \frac{1}{2}\left(p_1^\nu B_1(p_1,m_0,m_1) + p_{21}^\nu B_1(p_{21},m_1,m_2) + p_1^\nu B(p_{21},m_1,m_2)\right. \\ & \left. -\frac{1}{2}p_1^\nu f_2 C_1 - \frac{1}{2}p_2^\nu f_2 C_2\right) , \end{aligned} \tag{A.21}$$

and third equation

$$\eta_{\mu\nu}C^{\mu\nu} = B_0(p_{21}, m_1, m_2) + m_0^2 C_0(p_1, p_2, m_0, m_1, m_2)\,. \tag{A.22}$$

A comparison of the coefficients of p_1^ν and p_2^ν gives five of the three equations above.

$$\begin{aligned}
C_{00} + p_1^2 C_{11} + p_1 \cdot p_2 C_{12} =& \frac{1}{2}\left(B_0(p_{21}, m_1, m_2) + B_1(p_{21}, m_1, m_2) - f_1 C_1\right)\\
p_1^2 C_{12} + p_1 \cdot p_2 C_{22} =& \frac{1}{2}\left(B_1(p_2, m_0, m_2) - B_1(p_{21}, m_1, m_2) - f_1 C_2\right)\\
p_1 \cdot p_2 C_{11} + p_2^2 C_{12} =& \frac{1}{2}\left(B_1(p_1, m_0, m_1) + B_1(p_{21}, m_1, m_2) + B_0(p_{21}, m_1, m_2) - f_2 C_1\right)\\
C_{00} + p_1 \cdot p_2 C_{12} + p_2^2 C_{22} =& -\frac{1}{2}\left(B_1(p_{21}, m_1, m_2) + f_2 C_2\right)\\
4C_{00} + p_1^2 C_{11} + 2p_1 \cdot p_2 C_{12} + p_2^2 C_{22} =& B_0(p_{21}, m_1, m_2) + m_0^2 C_0(p_1, p_2, m_0, m_1, m_2)\,.
\end{aligned} \tag{A.23}$$

From this system of linear equations and with the previous result we have everything we need for the gluon-fusion process.

B. Calculation of the three-point scalar function

There are many ways to calculate a scalar loop integral, e.g., using the Cutkosky cutting rule [47], Feynman parametrization, etc. In almost every quantum field theory textbook [48], [49] the Feynman trick is taught. In this appendix, we give a brief review of it. The first step is to introduce a further integral for every propagator, which yields

$$\begin{aligned} C_0 &= \int \frac{d^4q}{i\pi^2} \frac{1}{((q+p_1+p_2)^2 - m^2 + i\epsilon)(q^2 - m^2 + i\epsilon)((q+p_1)^2 - m^2 + i\epsilon)} \\ &= \int \frac{d^4q}{i\pi^2} \int_0^1 dx \int_0^1 dy \int_0^1 dz \\ &\quad \frac{2\delta(x+y+z-1)}{[x((q+p_1+p_2)^2 - m^2 + i\epsilon) + y(q^2 - m^2 + i\epsilon) + z((q+p_1)^2 - m^2 + i\epsilon)]^3} \,. \end{aligned} \tag{B.1}$$

Using the relations $x + y + z = 1$ which is a consequence of the Dirac delta function, $p_1^2 = p_2^2 = 0$ according to massless gluons and $2p_1 \cdot p_2 = m_H^2$ is the center of mass energy. The denominator of the loop integral can be expressed by

$$\begin{aligned} D &= x((q+p_1+p_2)^2 - m^2 + i\epsilon) + y(q^2 - m^2 + i\epsilon) + z((q+p_1)^2 - m^2 + i\epsilon) \\ &= q^2 + 2q(xp_1 + xp_2 + zp_1) + 2xp_1 \cdot p_2 - m^2 + i\epsilon \\ &= l^2 - \Delta + i\epsilon \,. \end{aligned} \tag{B.2}$$

In the last step, the variable $l = q + xp_1 + xp_2 + zp_1$ is introduced as the result of a linear variable tranformation, and $\Delta = (xp_1 + xp_2 + zp_1)^2 - 2xp_1 \cdot p_2 + m^2$ is the rest term. Substituting this in Eq. (B.1) and performing the y integral, results in

$$C_0 = 2 \int \frac{d^4l}{2\pi^2} \int_0^1 dx \int_0^{1-x} dz \, \frac{1}{(l^2 - \Delta + i\epsilon)^3} \,. \tag{B.3}$$

There is another trick for getting rid of the ϵ-term: the so-called Wick-rotation. The space components are rotated such that the integral becomes Euclidian. Using spherical coordinates and performing the integrals, Ep. (B.3) reads

$$\begin{aligned} C_0 &= \frac{2i}{(-1)^3} \int \frac{dl_E \, d\Omega}{i\pi^2} \int_0^1 dx \int_0^{1-x} dz \, \frac{l_E^3}{(l_E^2 + \Delta)^3} \\ &= \frac{2i}{(-1)^3} \frac{2\pi^2}{i\pi^2} \int_0^1 dx \int_0^{1-x} dz \, \frac{1}{4\Delta} \, . \end{aligned} \tag{B.4}$$

At this stage, only the last two Feynman parameter integrals are left. The z integral is pretty easy to calculate, but the general solution for the x integral is a dilogarithm. Taking advantage of dilogarithms relations, the final result is [46]

$$\begin{aligned} C_0 &= -\int_0^1 dx \int_0^{1-x} dz \, \frac{1}{m_H^2 x(x+z-1) + m^2} \\ &= \int_0^1 \frac{dx}{m_H^2 x} \log\left(\frac{m_H^2 x(1-x) - m^2}{-m_H^2 x^2 - m^2} \right) \\ &= \frac{1}{2m_H^2} \log\left(-\frac{1 + \sqrt{1 - \frac{4m^2}{m_H^2}}}{1 - \sqrt{1 - \frac{4m^2}{m_H^2}}} \right) \, . \end{aligned} \tag{B.5}$$

C. Mass eigenstates

In the mixing case, there appear terms that are proportional to the product of the two Higgs fields which leads to a non diagonal mass mixing matrix. For this reason, this matrix must be diagonalised to get the mass eigenstates. The mass mixing matrix

$$M^2 = \begin{pmatrix} 2\lambda_s v_s & \eta_x v_s v_h \\ \eta_x v_s v_h & 2\lambda_h v_h \end{pmatrix} \tag{C.1}$$

is symmetric. Thus, it has real eigenvalues and the corresponding eigenvectors are orthogonal to each other. A matrix S that transforms the mass mixing matrix M^2 to a diagonal matrix M_D^2

$$M^2 = S^T M_D^2 S\,, \tag{C.2}$$

which matrix elements are the eigenvalues m_1 and m_2

$$M_D^2 = \begin{pmatrix} m_1^2 & 0 \\ 0 & m_2^2 \end{pmatrix}\,, \tag{C.3}$$

and vice versa, can be constructed from the eigenvectors. Hence, the first step is to calculate the eigenvalues from Eq. (C.1). The equation that defines the eigenvalues is a homogenous system of linear equation. By taking the determinant of this equation,

$$\det(M^2 - m^2) = (2\lambda_s v_s^2 - m^2)(2\lambda_s v_s^2 - m^2) - (\eta_x v_s v_h)^2 = 0\,, \tag{C.4}$$

leads to the characteristic polynomial

$$m^2 - 2m(\lambda_s v_s^2 + \lambda_h v_h^2) + 4\lambda_s v_s^2 \lambda_h v_h^2 - (\eta_x v_s v_h)^2 = 0\,. \tag{C.5}$$

The roots of the equation are the eigenvalues

$$\begin{aligned} m_{1,2}^2 &= \lambda_s v_s^2 + \lambda_h v_h^2 \pm \sqrt{(\lambda_s v_s^2 + \lambda_h v_h^2)^2 - 4\lambda_s v_s^2 \lambda_h v_h^2 + (\eta_x v_s v_h)^2} \\ &= \lambda_s v_s^2 + \lambda_h v_h^2 \pm \sqrt{(\lambda_s v_s^2 - \lambda_h v_h^2)^2 + (\eta_x v_s v_h)^2}\,. \end{aligned} \tag{C.6}$$

With the help of MATHEMATICA and the abbreviation

$$x = \frac{m_1^2 - 2\lambda_h v_h^2}{\eta_x v_s v_h}\,, \tag{C.7}$$

the solution of S is given by

$$S = \begin{pmatrix} \frac{x}{\sqrt{1+x^2}} & \frac{1}{\sqrt{1+x^2}} \\ -\frac{1}{\sqrt{1+x^2}} & \frac{x}{\sqrt{1+x^2}} \end{pmatrix} = \begin{pmatrix} \cos\chi & \sin\chi \\ -\sin\chi & \cos\chi \end{pmatrix}\,, \tag{C.8}$$

where χ is the mixing angle of the two Higgs bosons. The matrix S rotates the fields h_s and h_h to mass eigenstates h_1 and h_2. For the mixing angle χ, another equation can be derived

$$\tan 2\chi = \frac{\sin 2\chi}{\cos 2\chi} = \frac{2\sin\chi\cos\chi}{\cos^2\chi - \sin^2\chi} = \frac{\eta_x v_s v_h}{\lambda_s v_s^2 - \lambda_h v_h^2}. \tag{C.9}$$

Putting the mass eigenstates into Eq. (3.18) the Lagrangian for the self-interacting part reads

$$\begin{aligned} \mathscr{L}_{111} &= \frac{1}{2}(c_\chi s_\chi \eta_x (c_\chi v_h + s_\chi v_s) + 2s_\chi^3 \lambda_h v_h + 2c_\chi^3 \lambda_s v_s) h_1^3 \\ \mathscr{L}_{222} &= \frac{1}{2}(c_\chi s_\chi \eta_x (s_\chi v_h - c_\chi v_s) + 2c_\chi^3 \lambda_h v_h - 2s_\chi^3 \lambda_s v_s) h_2^3 \\ \mathscr{L}_{1111} &= \frac{1}{4}(c_\chi^2 s_\chi^2 \eta_x + c_\chi^4 \lambda_s + s_\chi^4 \lambda_h) h_1^4 \\ \mathscr{L}_{2222} &= \frac{1}{4}(c_\chi^2 s_\chi^2 \eta_x + s_\chi^4 \lambda_s + c_\chi^4 \lambda_h) h_2^4\,. \end{aligned} \tag{C.10}$$

And the interaction of the two fields can be written as

$$
\begin{aligned}
\mathscr{L}_{112} &= \frac{1}{2}(s_\chi \eta_x v_s (2c_\chi^2 - s_\chi^2) + c_\chi \eta_x v_h (c_\chi^2 - 2s_\chi^2) + 6c_\chi s_\chi (s_\chi \lambda_h v_h - c_\chi \lambda_s v_s)) h_1^2 h_2 \\
\mathscr{L}_{122} &= \frac{1}{2}(c_\chi \eta_x v_s (c_\chi^2 - 2s_\chi^2) + s_\chi \eta_x v_h (s_\chi^2 - 2c_\chi^2) + 6c_\chi s_\chi (s_\chi \lambda_s v_s + c_\chi \lambda_h v_h)) h_1 h_2^2 \\
\mathscr{L}_{1122} &= \frac{1}{4}(\eta_x (c_\chi^4 + s_\chi^4 - 4c_\chi^2 s_\chi^2) + 6c_\chi^2 s_\chi^2 (\lambda_s + \lambda_h)) h_1^2 h_2^2 \\
\mathscr{L}_{1112} &= \frac{1}{2} c_\chi s_\chi (\eta_x (c_\chi^2 - s_\chi^2) + 2s_\chi^2 \lambda_h - 2c_\chi^2 \lambda_s) h_1^3 h_2 \\
\mathscr{L}_{1222} &= \frac{1}{4} c_\chi s_\chi (\eta_x (s_\chi^2 - c_\chi^2) + 2c_\chi^2 \lambda_h - 2s_\chi^2 \lambda_s) h_1 h_2^3
\end{aligned}
\tag{C.11}
$$

with the abbreviation

$$
c_\chi = \cos\chi\,, \quad s_\chi = \sin\chi\,. \tag{C.12}
$$

Starting from these Lagrangians, the Feynman rules are shown in App. D.

D. Feynman rules for the hidden Higgs portal model

In this appendix all Feynman rules of the hidden Higgs model are listed. By defining the abbreviations for the coupling constants of the self-interaction vertices

$$\begin{aligned}
\eta_{111} &= c_\chi s_\chi \eta_x (c_\chi v_h + s_\chi v_s) + 2 s_\chi^3 \lambda_h v_h + 2 c_\chi^3 \lambda_s v_s \\
\eta_{222} &= c_\chi s_\chi \eta_x (s_\chi v_h - c_\chi v_s) + 2 c_\chi^3 \lambda_h v_h - 2 s_\chi^3 \lambda_s v_s \\
\eta_{1111} &= c_\chi^2 s_\chi^2 \eta_x + c_\chi^4 \lambda_s + s_\chi^4 \lambda_h \\
\eta_{2222} &= c_\chi^2 s_\chi^2 \eta_x + s_\chi^4 \lambda_s + c_\chi^4 \lambda_h \,,
\end{aligned} \tag{D.1}$$

and the interaction between the two fields

$$\begin{aligned}
\eta_{112} &= s_\chi \eta_x v_s (2 c_\chi^2 - s_\chi^2) + c_\chi \eta_x v_h (c_\chi^2 - 2 s_\chi^2) + 6 c_\chi s_\chi (s_\chi \lambda_h v_h - c_\chi \lambda_s v_s) \\
\eta_{122} &= c_\chi \eta_x v_s (c_\chi^2 - 2 s_\chi^2) + s_\chi \eta_x v_h (s_\chi^2 - 2 c_\chi^2) + 6 c_\chi s_\chi (s_\chi \lambda_s v_s + c_\chi \lambda_h v_h) \\
\eta_{1122} &= \eta_x (c_\chi^4 + s_\chi^4 - 4 c_\chi^2 s_\chi^2) + 6 c_\chi^2 s_\chi^2 (\lambda_s + \lambda_h) \\
\eta_{1112} &= c_\chi s_\chi (\eta_x (c_\chi^2 - s_\chi^2) + 2 s_\chi^2 \lambda_h - 2 c_\chi^2 \lambda_s) \\
\eta_{1222} &= c_\chi s_\chi (\eta_x (s_\chi^2 - c_\chi^2) + 2 c_\chi^2 \lambda_h - 2 s_\chi^2 \lambda_s) \,,
\end{aligned} \tag{D.2}$$

the Feynman rules can be read off from Eqs. (C.10) and (C.11) without much afford except of prefactors. In the limit when the sine of the mixing angle goes to zero, the mixing case degenerates to the scalar case. If additionally $h_2 = 0$, only the standard model is left.

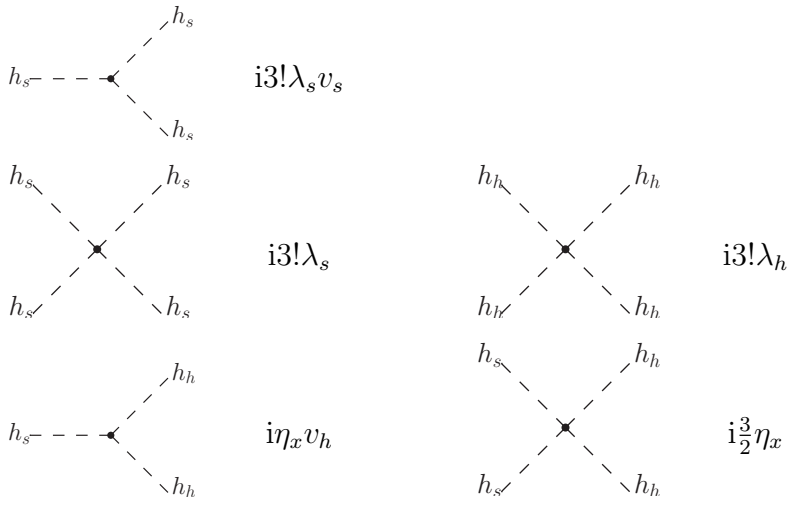

Table D.1.: These are the Feynman rules in the scalar case. The minimal SM Higgs sector is extended by only three further interactions. The vertices where only SM Higgs appears are the same.

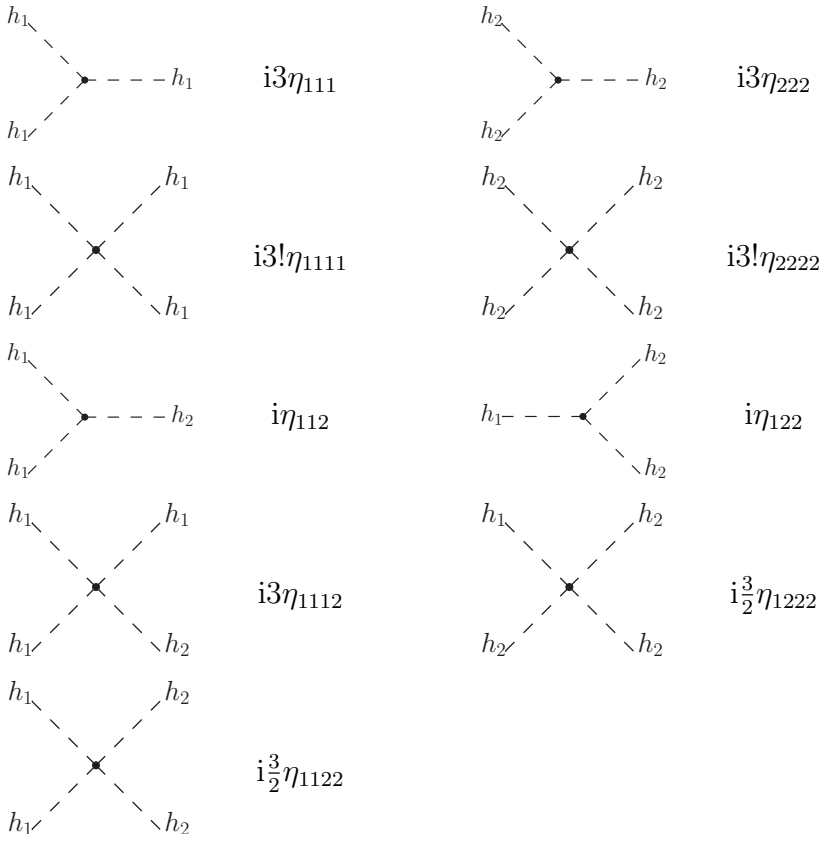

Table D.2.: These are the Feynman rules in the mixing case where only Higgs bosons appear. In comparison to the scalar case, much more vertices are possible.

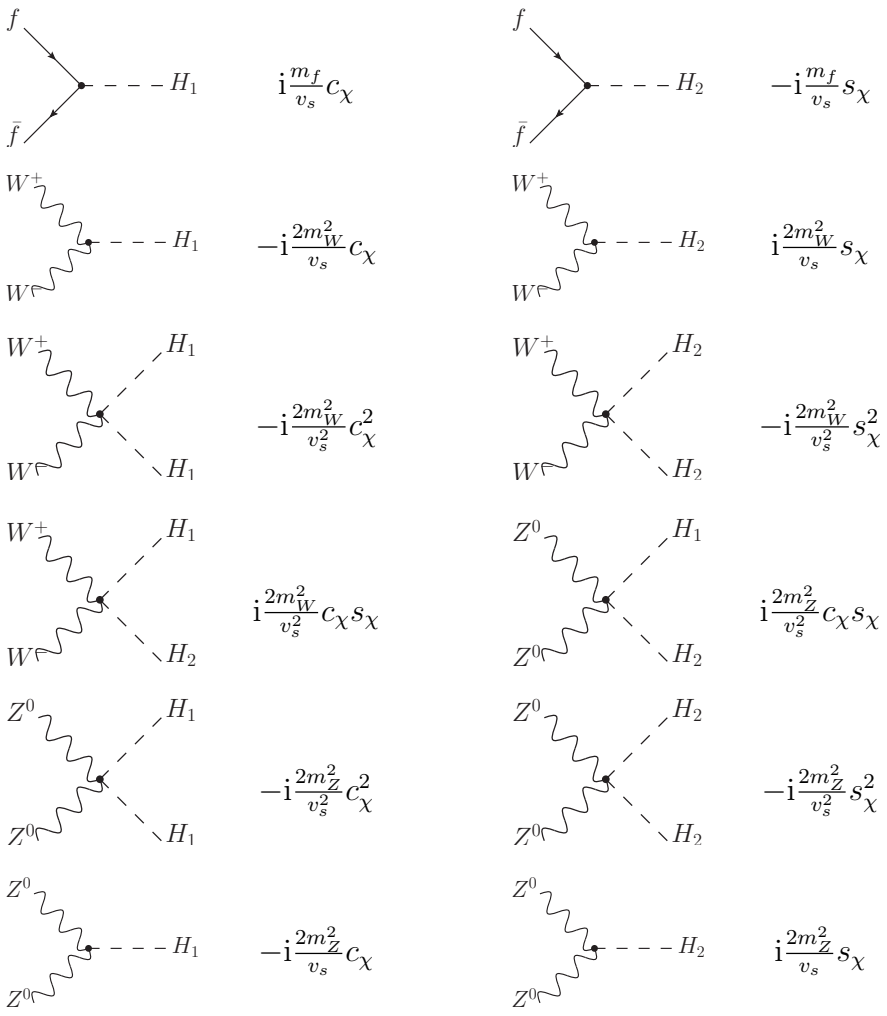

Table D.3.: These are the Feynman rules in the mixing case where the Higgs bosons interact with fermions and weak gauge bosons. Also the hidden Higgs boson interacts with the SM particles because of the mass mixing.

E. Observational bias

Statistical fluctuations in the measurements can lead to situations which cannot be interpreted in terms of physically meaningful parameters. One such example is a negative number of signal events. At the LHC we first measure the sum of signal and background events in the signal region. The number of background events we then determine either from extrapolation from a signal-free control region, like sidebands, or from Monte Carlo simulations. The difference gives us the number of signal events. At arbitrarily large statistical significances the difference between the two measurements, *i.e.* the number of signal events, is by definition much larger than the statistical error on each of them individually. However, for significances between one and three standard deviations as we expect them for the Higgs sector at the LHC a downward fluctuation in signal-plus-background and an upward fluctuation in background-only can lead to a negative difference. This effect has to be dealt with when we compose the sample of measurements which for example enter the Higgs sector analysis presented in this paper. The question is, if solutions to this problem will affect for example the central values and errors quoted for the Higgs couplings.

We present three alternative treatments in Figure E.1. On the left-hand side we only take into account channels where we measure a positive number of signal events. This prescription we use in our analysis. For couplings fairly close to their Standard Model values we obtain the correct central value. For small couplings we observe a significant shift to larger values. The reason is that if a measurement shows an upward signal fluctuation we include it, while a downward fluctuation quickly reaches the negative-S threshold and gets excluded.

In the central panel we only include measurements where the nominal number of signal and background events yields a 2σ excess. We find good agreement between fitted and truth values of χ, but for $\cos^2\chi < 0.7$ there are no measurements left which fulfill this condition.

For the right panel we only include channels where the measured numbers yield a 2σ excess. Here, we observe a significant upward shift over the whole parameter range. Even for Standard Model couplings the actual Standard Model is almost excluded at the 95% CL. Therefore, it is important to take into account measurements which have a low observed significance on their own. They can provide upper bounds on Higgs couplings and avoid a bias generated by upward fluctuations of signal events in some of the channels included.

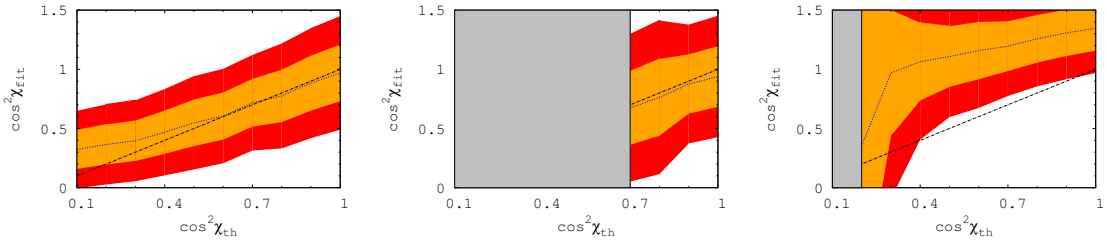

Figure E.1.: Different treatment of channels, depending on the number of events in the signal region $S + B$, compared to background events B from a signal-free control region. Left: a measurement is included when $S + B > B$. Center: only measurements corresponding to at least a 2σ excess for nominal signal and background rates are included. Right: only measurements for which the measured values of $S + B$ and B give at least two standard deviations are included.

F. Scaling of cross sections in a strongly-interacting Higgs scenario

For the un-aligned shifts of Higgs-gauge and Yukawa couplings the scaling of the cross sections with ξ does not follow a simple pattern. However, the main features can be illustrated for two characteristic leading channels, Higgs-strahlung $q\bar{q}' \to WH, H \to b\bar{b}$, and gluon-fusion $gg \to H \to \gamma\gamma$. Ignoring resummation effects in this qualitative discussion, the corresponding scaling functions, normalized to unity at the Standard Model value $\xi = 0$, can be approximated as

$$\begin{aligned}
\left(\frac{N_{\rm ev}}{N_{\rm ev}^{\rm SM}}\right)_{WH,bb} &= \frac{1}{\mathcal{N}_{WH,bb}} \frac{(1-\xi)\,\dfrac{(1-2\xi)^2}{(1-\xi)}}{\dfrac{(1-2\xi)^2}{(1-\xi)} + \gamma(1-\xi)} \\
\left(\frac{N_{\rm ev}}{N_{\rm ev}^{\rm SM}}\right)_{gg,\gamma\gamma} &= \frac{1}{\mathcal{N}_{gg,\gamma\gamma}} \frac{\dfrac{(1-2\xi)^2}{(1-\xi)}\left[\dfrac{(1-2\xi)^2}{(1-\xi)} + \beta_1(1-2\xi) + \beta_2(1-\xi)\right]}{\dfrac{(1-2\xi)^2}{(1-\xi)} + \gamma(1-\xi)} \,.
\end{aligned} \tag{F.1}$$

The parameter $\gamma \sim 0.05$ accounts for the admixture of $H \to WW$ and ZZ decays compared to $H \to b\bar{b}$ for Higgs masses close to 120 GeV while $\beta_{1,2} \sim -8.9$, 19.8 parametrize top- and W-loop contributions for Higgs decays to photons, including their destructive interference.

As shown in Fig. F.1 the scaling function for Higgs-strahlung plus $b\bar{b}$ decays falls off straight, apart from a narrow well close to $\xi = 0.5$. There, the rates for observing a Higgs boson are driven to zero. The scaling function for gluon fusion and $\gamma\gamma$ decay behaves similarly, except above the well, where the scaling function diverges for $\xi \to 1$. The multiplicities of the solutions are illustrated for $\xi = 0.2$ and $\xi = 0.6$ by the two dashed lines. Depending on the value of ξ, either one or up to three solutions correspond to given values of the scaling functions. By combining the two sets of the solutions for the two channels the individual ambiguities are resolved: the fake solutions for ξ (open circles) are eliminated and only the true value (full circle) remains.

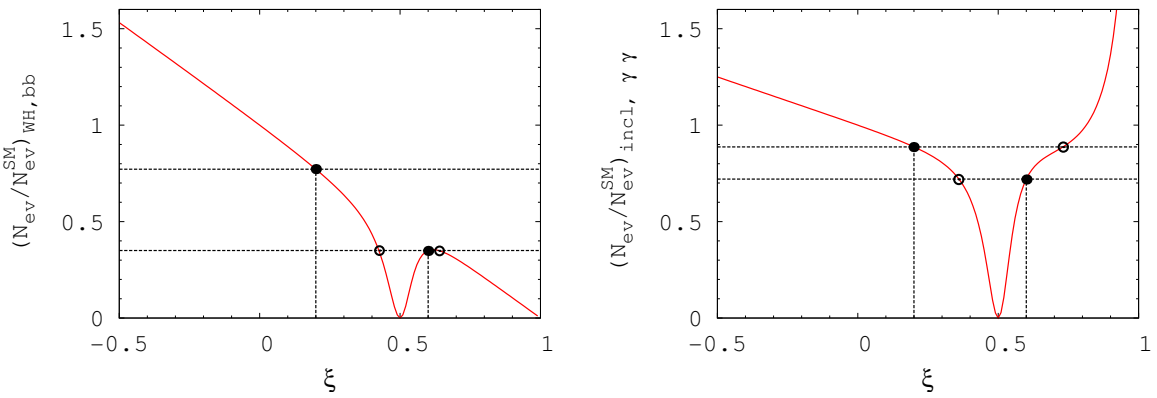

Figure F.1.: The scaling functions for Higgs-strahlung $WH, H \to b\bar{b}$ and gluon fusion $gg \to H \to \gamma\gamma$. The full circle on the straight lines marks the true unique solution, while the open circles denote fake values which are different for the two channels.

This theoretical picture is realized only for large event numbers. Otherwise, remnants of the fake solutions cannot be eliminated completely. This is illustrated in Fig. F.2 where we present the log-likelihood bands for ξ. In the upper panels we show the individual Higgs-strahlung and gluon-fusion channels, including their individual fake solutions. In the lower panels we first combine the two channels, strongly reducing the fake solutions. In the bottom right panel we include all available channels, eliminating entirely the fake solutions. Only the width around the true value in two preferred directions remains.

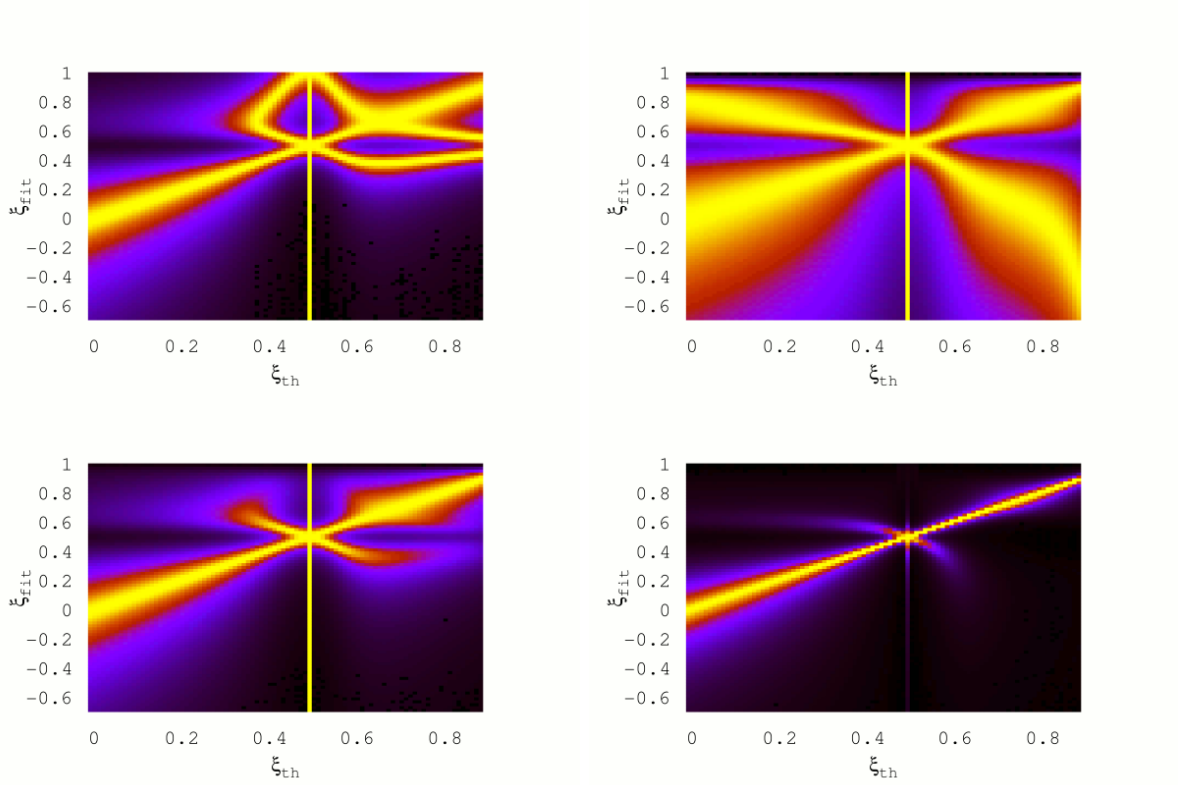

Figure F.2.: Extracted values for ξ as a function of the assumed ξ_{th} for $M_H = 120$ GeV and 30 fb^{-1}. We show profile likelihoods, where we have neglected theory errors for clarity. Upper: Higgs-strahlung plus $b\bar{b}$ decay (left), and gluon fusion plus $\gamma\gamma$ decay (right). Lower: Combination of the two channels (left) and including all available channels (right).

Bibliography

[1] P. W. Higgs, "Broken symmetries, massless particles and gauge fields," Phys. Lett. **12** (1964) 132.

[2] P. W. Higgs, "BROKEN SYMMETRIES AND THE MASSES OF GAUGE BOSONS," Phys. Rev. Lett. **13** (1964) 508.

[3] F. Englert and R. Brout, "BROKEN SYMMETRY AND THE MASS OF GAUGE VECTOR MESONS," Phys. Rev. Lett. **13** (1964) 321.

[4] G. S. Guralnik, C. R. Hagen and T. W. B. Kibble, "GLOBAL CONSERVATION LAWS AND MASSLESS PARTICLES," Phys. Rev. Lett. **13** (1964) 585.

[5] S. Weinberg, "A Model Of Leptons," Phys. Rev. Lett. **19** (1967) 1264.

[6] S. L. Glashow, "Partial Symmetries Of Weak Interactions," Nucl. Phys. **22** (1961) 579.

[7] A. Salam and J. C. Ward, "Electromagnetic and weak interactions," Phys. Lett. **13** (1964) 168.

[8] R. Barate *et al.* [LEP Working Group for Higgs boson searches and ALEPH Collaboration and and], "Search for the standard model Higgs boson at LEP," Phys. Lett. B **565** (2003) 61 [arXiv:hep-ex/0306033].

[9] T. P. Cheng, E. Eichten and L. F. Li, "Higgs Phenomena In Asymptotically Free Gauge Theories," Phys. Rev. D **9** (1974) 2259.

[10] N. Cabibbo, L. Maiani, G. Parisi and R. Petronzio, "Bounds On The Fermions And Higgs Boson Masses In Grand Unified Theories," Nucl. Phys. B **158** (1979) 295.

[11] T. Hambye and K. Riesselmann, "Matching conditions and Higgs mass upper bounds revisited," Phys. Rev. D **55** (1997) 7255 [arXiv:hep-ph/9610272].

[12] M. Lindner, M. Sher and H. W. Zaglauer, "Probing Vacuum Stability Bounds At The Fermilab Collider," Phys. Lett. B **228** (1989) 139.

[13] H. E. Haber, G. L. Kane and T. Sterling, "The Fermion Mass Scale And Possible Effects Of Higgs Bosons On Experimental Observables," Nucl. Phys. B **161** (1979) 493.

[14] J. F. Donoghue and L. F. Li, "Properties Of Charged Higgs Bosons," Phys. Rev. D **19** (1979) 945.

[15] T. P. Cheng and M. Sher, "Mass Matrix Ansatz and Flavor Nonconservation in Models with Multiple Higgs Doublets," Phys. Rev. D **35** (1987) 3484.

[16] A. Einstein, "On the electrodynamics of moving bodies," Annalen Phys. **17** (1905) 891 [Annalen Phys. **14** (2005) 194].

[17] A. Einstein, "The foundation of the general theory of relativity," Annalen Phys. **49** (1916) 769 [Annalen Phys. **14** (2005) 517].

[18] M. Milgrom, "A Modification Of The Newtonian Dynamics As A Possible Alternative To The Hidden Mass Hypothesis," Astrophys. J. **270** (1983) 365.

[19] T. Gehrels, "The multiverse and the origin of our universe," arXiv:0707.1030 [astro-ph].

[20] A. G. Riess *et al.* [Supernova Search Team Collaboration], "Observational Evidence from Supernovae for an Accelerating Universe and a Cosmological Constant," Astron. J. **116** (1998) 1009 [arXiv:astro-ph/9805201].

[21] N. Arkani-Hamed, S. Dimopoulos and G. R. Dvali, "The hierarchy problem and new dimensions at a millimeter," Phys. Lett. B **429** (1998) 263 [arXiv:hep-ph/9803315].

[22] L. Randall and R. Sundrum, "An alternative to compactification," Phys. Rev. Lett. **83** (1999) 4690 [arXiv:hep-th/9906064].

[23] J. M. Maldacena, "The large N limit of superconformal field theories and supergravity," Adv. Theor. Math. Phys. **2** (1998) 231 [Int. J. Theor. Phys. **38** (1999) 1113] [arXiv:hep-th/9711200].

[24] J. Wess and B. Zumino, "Supergauge Transformations in Four-Dimensions," Nucl. Phys. B **70** (1974) 39.

[25] J. A. M. Vermaseren, "The Symbolic manipulation program FORM,"

[26] J. A. M. Vermaseren, "New features of FORM," arXiv:math-ph/0010025.

[27] A. Djouadi, J. Kalinowski and M. Spira, "HDECAY: A program for Higgs boson decays in the standard model and its supersymmetric extension," Comput. Phys. Commun. **108** (1998) 56 [arXiv:hep-ph/9704448].

[28] T. Plehn, M. Spira and P. M. Zerwas, "Pair Production of Neutral Higgs Particles in Gluon–Gluon Collisions," Nucl. Phys. B **479** (1996) 46 [Erratum-ibid. B **531** (1998) 655] [arXiv:hep-ph/9603205].

[29] M. Perelstein, "Introduction to Collider Physics," arXiv:1002.0274 [hep-ph].

[30] T. Gleisberg, S. Hoche, F. Krauss, A. Schalicke, S. Schumann and J. C. Winter, "SHERPA 1.alpha, a proof-of-concept version," JHEP **0402** (2004) 056 [arXiv:hep-ph/0311263].

[31] T. Sjostrand, S. Mrenna and P. Z. Skands, "PYTHIA 6.4 Physics and Manual," JHEP **0605** (2006) 026 [arXiv:hep-ph/0603175].

[32] W. Giele *et al.*, "The QCD / SM working group: Summary report," arXiv:hep-ph/0204316.

[33] A. D. Martin, R. G. Roberts, W. J. Stirling and R. S. Thorne, "Physical gluons and high E(T) jets," Phys. Lett. B **604** (2004) 61 [arXiv:hep-ph/0410230].

[34] C. Amsler *et al.* [Particle Data Group], "Review of particle physics," Phys. Lett. B **667** (2008) 1.

[35] M. J. Strassler, "Possible effects of a hidden valley on supersymmetric phenomenology," arXiv:hep-ph/0607160.

[36] K. M. Zurek, "Multi-Component Dark Matter," Phys. Rev. D **79** (2009) 115002 [arXiv:0811.4429 [hep-ph]].

[37] R. Blumenhagen, M. Cvetic, P. Langacker and G. Shiu, "Toward realistic intersecting D-brane models," Ann. Rev. Nucl. Part. Sci. **55** (2005) 71 [arXiv:hep-th/0502005].

[38] G. Cynolter, E. Lendvai and G. Pocsik, "Note on unitarity constraints in a model for a singlet scalar dark matter candidate," Acta Phys. Polon. B **36** (2005) 827 [arXiv:hep-ph/0410102].

[39] R. Lafaye, T. Plehn and D. Zerwas, "SFITTER: SUSY parameter analysis at LHC and LC," arXiv:hep-ph/0404282.

[40] M. Rauch, R. Lafaye, T. Plehn and D. Zerwas, "SFitter: Reconstructing the MSSM Lagrangian from LHC data," arXiv:0710.2822 [hep-ph].

[41] R. Lafaye, M. Rauch, T. Plehn and D. Zerwas, "Sfitter: Determining Supersymmetric Parameters,"

[42] C. Adam, J. L. Kneur, R. Lafaye, T. Plehn, M. Rauch and D. Zerwas, "Measuring Unification," arXiv:1007.2190 [hep-ph].

[43] S. Bock, R. Lafaye, T. Plehn, M. Rauch, D. Zerwas and P. M. Zerwas, "Measuring Hidden Higgs and Strongly-Interacting Higgs Scenarios," arXiv:1007.2645 [hep-ph].

[44] G. Passarino and M. J. G. Veltman, "One Loop Corrections For E+ E- Annihilation Into Mu+ Mu- In The Weinberg Model," Nucl. Phys. B **160** (1979) 151.

[45] R. Mertig, M. Bohm and A. Denner, "FEYN CALC: Computer algebraic calculation of Feynman amplitudes," Comput. Phys. Commun. **64** (1991) 345.

[46] B. A. Kniehl, "ON THE DECAY MODE $Z \to H$ g g," Phys. Rev. D **42** (1990) 3100.

[47] R. E. Cutkosky, "Singularities and discontinuities of Feynman amplitudes," J. Math. Phys. **1** (1960) 429.

[48] Michael E. Peskin, Daniel V. Schroeder, "An Introduction to Quantum Field Theory", Perseus Books 1995

[49] Mark Srednicki, "Quantum Field Theory", Cambridge University Press 2007

[50] Cliff Burgess, Guy Moore, "The Standard Model: A Primer", Cambridge University Press 2006

[51] William H. Press, Saul A. Teukolsky, William T. Vetterling, Brian P. Flannery, "Numerical Recipes: The Art of Scientific Computing", Cambridge University Press 2007

[52] R. K. Ellis, W. J. Stirling, B. R. Webber, "QCD and Collider Physics", Cambridge University Press 2003

[53] Ilja Bronstein, Konstantin A. Semendjajew, Gerhard Musiol, Heiner Muehlig, "Taschenbuch der Mathematik", Harri Deutsch 2000

[54] A. Djouadi, "The Anatomy of electro-weak symmetry breaking. I: The Higgs boson in the standard model," Phys. Rept. **457**, 1 (2008); [arXiv:hep-ph/0503172];

[55] A. Djouadi, "The Anatomy of electro-weak symmetry breaking. II. The Higgs bosons in the minimal supersymmetric model," Phys. Rept. **459**, 1 (2008). [arXiv:hep-ph/0503173].

[56] M. Spira, "QCD effects in Higgs physics," Fortsch. Phys. **46**, 203 (1998); [arXiv:hep-ph/9705337];

[57] V. Buescher and K. Jakobs, "Higgs boson searches at hadron colliders," Int. J. Mod. Phys. A **20**, 2523 (2005); [arXiv:hep-ph/0504099];

[58] D. Rainwater, "Searching for the Higgs boson," [arXiv:hep-ph/0702124];

[59] M. Gomez-Bock, M. Mondragon, M. Muhlleitner, M. Spira and P. M. Zerwas, "Concepts of Electroweak Symmetry Breaking and Higgs Physics," [arXiv:0712.2419 [hep-ph]];

[60] J. D. Wells, "Lectures on Higgs Boson Physics in the Standard Model and Beyond," [arXiv:0909.4541 [hep-ph]];

[61] T. Plehn, "An LHC Lecture," [arXiv:0910.4182 [hep-ph]].

[62] M. Duhrssen, S. Heinemeyer, H. Logan, D. Rainwater, G. Weiglein and D. Zeppenfeld, "Extracting Higgs boson couplings from LHC data," Phys. Rev. D **70**, 113009 (2004). [arXiv:hep-ph/0406323].

[63] R. Lafaye, T. Plehn, M. Rauch, D. Zerwas and M. Duhrssen, "Measuring the Higgs Sector," JHEP **0908**, 009 (2009). [arXiv:0904.3866 [hep-ph]].

[64] R. Barbieri, T. Gregoire and L. J. Hall, "Mirror world at the Large Hadron Collider," arXiv:hep-ph/0509242;

[65] M. J. Strassler and K. M. Zurek, "Echoes of a hidden valley at hadron colliders," Phys. Lett. B **651**, 374 (2007); [arXiv:hep-ph/0604261].

[66] B. Patt and F. Wilczek, "Higgs-field portal into hidden sectors," arXiv:hep-ph/0605188;

[67] M. J. Strassler and K. M. Zurek, "Discovering the Higgs through highly-displaced vertices," Phys. Lett. B **661**, 263 (2008). [arXiv:hep-ph/0605193].

[68] M. Bowen, Y. Cui and J. D. Wells, "Narrow trans-TeV Higgs bosons and H –> h h decays: Two LHC search paths for a hidden sector Higgs boson," JHEP **0703** (2007) 036; [arXiv:hep-ph/0701035].

[69] V. Barger, P. Langacker, M. McCaskey, M. J. Ramsey-Musolf and G. Shaughnessy, "LHC Phenomenology of an Extended Standard Model with a Real Scalar Singlet," Phys. Rev. D **77**, 035005 (2008). [arXiv:0706.4311 [hep-ph]].

[70] T. Binoth and J. J. van der Bij, "Influence of strongly coupled, hidden scalars on Higgs signals," Z. Phys. C **75**, 17 (1997) [arXiv:hep-ph/9608245].

[71] D. E. Morrissey, T. Plehn and T. M. P. Tait, "New Physics at the LHC," arXiv:0912.3259 [hep-ph].

[72] D. B. Kaplan, H. Georgi and S. Dimopoulos, "Composite Higgs Scalars," Phys. Lett. B **136**, 187 (1984);

[73] H. Georgi and D. B. Kaplan, "Composite Higgs And Custodial SU(2)," Phys. Lett. B **145**, 216 (1984);

[74] H. Georgi, D. B. Kaplan and P. Galison, "Calculation Of The Composite Higgs Mass," Phys. Lett. B **143**, 152 (1984).

[75] G. F. Giudice, C. Grojean, A. Pomarol and R. Rattazzi, "The Strongly-Interacting Light Higgs," JHEP **0706**, 045 (2007); [arXiv:hep-ph/0703164];

[76] I. Low, R. Rattazzi and A. Vichi, "Theoretical Constraints on the Higgs Effective Couplings," JHEP **1004**, 126 (2010). [arXiv:0907.5413 [hep-ph]].

[77] T. Han, D. Krohn, L. T. Wang and W. Zhu, "New Physics Signals in Longitudinal Gauge Boson Scattering at the LHC," JHEP **1003**, 082 (2010); [arXiv:0911.3656 [hep-ph]].

[78] R. Contino, C. Grojean, M. Moretti, F. Piccinini and R. Rattazzi, "Strong Double Higgs Production at the LHC," JHEP **1005**, 089 (2010). [arXiv:1002.1011 [hep-ph]].

[79] J. R. Espinosa, C. Grojean and M. Muhlleitner, "Composite Higgs Search at the LHC," JHEP **1005**, 065 (2010). [arXiv:1003.3251 [hep-ph]].

[80] W. Buchmuller and D. Wyler, "Effective Lagrangian Analysis Of New Interactions And Flavor Conservation," Nucl. Phys. B **268**, 621 (1986);

[81] K. Hagiwara, R. Szalapski and D. Zeppenfeld, "Anomalous Higgs Boson Production And Decay," Phys. Lett. B **318**, 155 (1993). [arXiv:hep-ph/9308347].

[82] T. Plehn, D. L. Rainwater and D. Zeppenfeld, "Determining the structure of Higgs couplings at the LHC," Phys. Rev. Lett. **88**, 051801 (2002); [arXiv:hep-ph/0105325].

[83] V. Hankele, G. Klamke, D. Zeppenfeld and T. Figy, "Anomalous Higgs boson couplings in vector boson fusion at the CERN LHC," Phys. Rev. D **74**, 095001 (2006); [arXiv:hep-ph/0609075].

[84] C. Ruwiedel, N. Wermes and M. Schumacher, "Prospects for the measurement of the structure of the coupling of a Higgs boson to weak gauge bosons in weak boson fusion with the ATLAS detector," Eur. Phys. J. C **51**, 385 (2007).

[85] J. R. Dell'Aquila and C. A. Nelson, "P Or CP Determination By Sequential Decays: V1 V2 Modes With Decays Into Anti-Lepton (A) Lepton (B) And/Or Anti-Q (A) Q (B)," Phys. Rev. D **33**, 80 (1986);

[86] C. A. Nelson, "CORRELATION BETWEEN DECAY PLANES IN HIGGS BOSON DECAYS INTO W PAIR (INTO Z PAIR)," Phys. Rev. D **37**, 1220 (1988);

[87] B. Field, "Distinguishing scalar from pseudoscalar Higgs production at the LHC," Phys. Rev. D **66**, 114007 (2002); [arXiv:hep-ph/0208262].

[88] D. J. . Miller, S. Y. Choi, B. Eberle, M. M. Muhlleitner and P. M. Zerwas, "Measuring the spin of the Higgs boson," Phys. Lett. B **505**, 149 (2001); [arXiv:hep-ph/0102023].

[89] S. Y. Choi, D. J. . Miller, M. M. Muhlleitner and P. M. Zerwas, "Identifying the Higgs spin and parity in decays to Z pairs," Phys. Lett. B **553**, 61 (2003); [arXiv:hep-ph/0210077].

[90] Y. Gao, A. V. Gritsan, Z. Guo, K. Melnikov, M. Schulze and N. V. Tran, "Spin determination of single-produced resonances at hadron colliders," Phys. Rev. D **81**, 075022 (2010); [arXiv:1001.3396 [hep-ph]].

[91] A. De Rujula, J. Lykken, M. Pierini, C. Rogan and M. Spiropulu, "Higgs look-alikes at the LHC," arXiv:1001.5300 [hep-ph].

[92] K. Hagiwara, P. Konar, Q. Li, K. Mawatari and D. Zeppenfeld, "Graviton production with 2 jets at the LHC in large extra dimensions," JHEP **0804**, 019 (2008); [arXiv:0801.1794 [hep-ph]];

[93] K. Hagiwara, J. Kanzaki, Q. Li and K. Mawatari, "HELAS and MadGraph/MadEvent with spin-2 particles," Eur. Phys. J. C **56**, 435 (2008). [arXiv:0805.2554 [hep-ph]].

[94] V. Barger, T. Han, P. Langacker, B. McElrath and P. Zerwas, "Effects of genuine dimension-six Higgs operators," Phys. Rev. D **67**, 115001 (2003). [arXiv:hep-ph/0301097].

[95] O. J. P. Eboli and D. Zeppenfeld, "Observing an invisible Higgs boson," Phys. Lett. B **495**, 147 (2000); [arXiv:hep-ph/0009158];

[96] R. M. Godbole, M. Guchait, K. Mazumdar, S. Moretti and D. P. Roy, "Search for 'invisible' Higgs signals at LHC via associated production with gauge bosons," Phys. Lett. B **571**, 184 (2003). [arXiv:hep-ph/0304137].

[97] G. Aad *et al.* [The ATLAS Collaboration], "Expected Performance of the ATLAS Experiment - Detector, Trigger and Physics," arXiv:0901.0512 [hep-ex].

[98] G. L. Bayatian *et al.* [CMS Collaboration], "CMS technical design report, volume II: Physics performance," J. Phys. G **34**, 995 (2007).

[99] A. De Roeck *et al.*, "From the LHC to Future Colliders," Eur. Phys. J. C **66**, 525 (2010). [arXiv:0909.3240 [hep-ph]].

[100] J. M. Butterworth, A. R. Davison, M. Rubin and G. P. Salam, "Jet substructure as a new Higgs search channel at the LHC," Phys. Rev. Lett. **100**, 242001 (2008); [arXiv:0802.2470 [hep-ph]].

[101] T. Plehn, G. P. Salam and M. Spannowsky, "Fat Jets for a Light Higgs," Phys. Rev. Lett. **104**, 111801 (2010). [arXiv:0910.5472 [hep-ph]].

[102] The ATLAS Collaboration, "ATLAS Sensitivity to the Standard Model Higgs in the HW and HZ Channels at High Transverse Momenta," ATL-PHYS-PUB-2009-088 (2009).

[103] A. Djouadi, M. Spira and P. M. Zerwas, "Production of Higgs bosons in proton colliders: QCD corrections," Phys. Lett. B **264** (1991) 440;

[104] S. Dawson, "Radiative corrections to Higgs boson production," Nucl. Phys. B **359** (1991) 283;

[105] M. Spira, A. Djouadi, D. Graudenz and P. M. Zerwas, "Higgs boson production at the LHC," Nucl. Phys. B **453** (1995) 17; [arXiv:hep-ph/9504378].

[106] R. V. Harlander and W. B. Kilgore, "Next-to-next-to-leading order Higgs production at hadron colliders," Phys. Rev. Lett. **88**, 201801 (2002);

[107] C. Anastasiou and K. Melnikov, "Higgs boson production at hadron colliders in NNLO QCD," Nucl. Phys. B **646**, 220 (2002);

[108] V. Ravindran, J. Smith and W. L. van Neerven, "NNLO corrections to the total cross section for Higgs boson production in hadron hadron collisions," Nucl. Phys. B **665**, 325 (2003); [arXiv:hep-ph/0302135].

[109] S. Moch and A. Vogt, "Higher-order soft corrections to lepton pair and Higgs boson production," Phys. Lett. B **631**, 48 (2005); [arXiv:hep-ph/0508265].

[110] A. Pak, M. Rogal and M. Steinhauser, "Finite top quark mass effects in NNLO Higgs boson production at LHC," JHEP **1002**, 025 (2010); [arXiv:0911.4662 [hep-ph]].

[111] R. V. Harlander, H. Mantler, S. Marzani and K. J. Ozeren, "Higgs production in gluon fusion at next-to-next-to-leading order QCD for finite top mass," Eur. Phys. J. C **66**, 359 (2010). [arXiv:0912.2104 [hep-ph]].

[112] T. Han, G. Valencia and S. Willenbrock, "Structure function approach to vector boson scattering in p p collisions," Phys. Rev. Lett. **69**, 3274 (1992); [arXiv:hep-ph/9206246].

[113] T. Figy, C. Oleari and D. Zeppenfeld, "Next-to-leading order jet distributions for Higgs boson production via weak-boson fusion," Phys. Rev. D **68**, 073005 (2003); [arXiv:hep-ph/0306109].

[114] M. Ciccolini, A. Denner and S. Dittmaier, "Strong and electroweak corrections to the production of Higgs+2jets via weak interactions at the LHC," Phys. Rev. Lett. **99**, 161803 (2007). [arXiv:0707.0381 [hep-ph]].

[115] M. Ciccolini, A. Denner and S. Dittmaier, "Electroweak and QCD corrections to Higgs production via vector-boson fusion at the LHC," Phys. Rev. D **77**, 013002 (2008); [arXiv:0710.4749 [hep-ph]].

[116] K. Arnold *et al.*, "VBFNLO: A parton level Monte Carlo for processes with electroweak bosons," Comput. Phys. Commun. **180**, 1661 (2009); [arXiv:0811.4559 [hep-ph]].

[117] P. Bolzoni, F. Maltoni, S. O. Moch and M. Zaro, "Higgs production via vector-boson fusion at NNLO in QCD," Phys. Rev. Lett. **105**, 011801 (2010). [arXiv:1003.4451 [hep-ph]].

[118] A. Djouadi, M. Spira and P. M. Zerwas, "QCD Corrections to Hadronic Higgs Decays," Z. Phys. C **70**, 427 (1996). [arXiv:hep-ph/9511344].

[119] A. Djouadi, J. Kalinowski and M. Spira, "HDECAY: A program for Higgs boson decays in the standard model and its supersymmetric extension," Comput. Phys. Commun. **108**, 56 (1998).

[120] A. Hocker, H. Lacker, S. Laplace and F. Le Diberder, "A New approach to a global fit of the CKM matrix," Eur. Phys. J. C **21**, 225 (2001). [arXiv:hep-ph/0104062].

[121] R. Lafaye, T. Plehn, M. Rauch and D. Zerwas, "Measuring Supersymmetry," Eur. Phys. J. C **54**, 617 (2008). [arXiv:0709.3985 [hep-ph]];

[122] N. Arkani-Hamed, M. Porrati and L. Randall, "Holography and phenomenology," JHEP **0108**, 017 (2001); [arXiv:hep-th/0012148].

[123] R. Rattazzi and A. Zaffaroni, "Comments on the holographic picture of the Randall-Sundrum model," JHEP **0104**, 021 (2001); [arXiv:hep-th/0012248].

[124] R. Contino, Y. Nomura and A. Pomarol, "Higgs as a holographic pseudo-Goldstone boson," Nucl. Phys. B **671**, 148 (2003); [arXiv:hep-ph/0306259].

[125] K. Agashe, R. Contino and A. Pomarol, "The Minimal Composite Higgs Model," Nucl. Phys. B **719**, 165 (2005); [arXiv:hep-ph/0412089].

[126] R. Contino, L. Da Rold and A. Pomarol, "Light custodians in natural composite Higgs models," Phys. Rev. D **75**, 055014 (2007). [arXiv:hep-ph/0612048].

Danksagung

Auch diese Arbeit ist nicht allein in Eigenregie entstanden, von daher wird es hier höchste Zeit allen Unterstützern gebührend zu danken. An erster Stelle möchte ich natürlich meinem Betreuer Herrn Prof. Dr. Tilman Plehn danken, weil er mir die Möglichkeit gab ein interessantes und auch sehr lehrreiches Thema zu bearbeiten.
Herrn Prof. Dr. Peter Zerwas möchte ich nicht nur für seine Idee für dieses Projekt danken sondern auch für seine stete Ansprechbarkeit und Hilfsbereitschaft während des ganzen Jahres. Seine ruhige und sachliche Art sorgte für eine angenehme und vertrauensvolle Zusammenarbeit.
Ebenso geht mein Dank an Herrn Dr. Michael Rauch für all seine Hilfe rund um SFitter. Ich denke, ich habe ihn in den letzten sechs Monaten so manches Mal zur Verzweiflung gebracht, aber seiner Geduld ist es geschuldet, dass die Arbeit noch abgeschlossen werden konnte. Bei meinen ersten Gehversuchen mit SFitter hat mich Herr Dr. Dirk Zerwas geleitet, weshalb ich ihm hier aufrichtig danken möchte.
Besonders in den ersten Monaten meiner Arbeit fand Herr Dr. Steffen Schumann bei Fragen zu C/C++ und Monte Carlo Methoden immer ein offenes Ohr. Desweiteren möchte ich noch den Herren Dr. Kentarou Mawatari, Dr. Michihisa Takeuchi und Dr. Christoph Englert für fruchtbare Gespräche und Anregungen danken.
Meinen beiden Bürokollegen Thomas Lübbert und Fabian Gross sei gedankt für die interessanten und lebhaften Diskussionen nicht nur physikalischer Natur.
Bei technischen und organisatorischen Problemen sowie Fragen zu LaTeX standen mir Konrad Schade und Matthias Kronenwett stets zur Seite. Zusammen mit Boris Nowak war immer für eine außerordentlich gute Stimmung gesorgt, die so manche schlechten Tage vergessen ließ.
An dieser Stelle möchte ich noch die Gelegenheit ergreifen, einem langen Weggefährten, Björn Sperling, zu danken. Nicht nur die Gespräche und gemeinsame Aktivitäten während unseres Physikstudium, das wir zusammen in Kiel aufgegriffen hatten, haben uns gegenseitig geprägt.
Meinen Eltern danke ich hier ganz besonders nicht nur für die finanzielle Unterstützung über viele Jahre sondern auch für ihr Verständnis für meine Berufswahl und deren Aufmunterung meinen Ideen nachzugehen.

最后我要感谢的是一个很特殊的人，也就是我的女朋友孙慧。因为她用她的爱，回护和理解，始终鼓励我。而当我偶有松懈，她也曾不吝严辞劝诫，促使我继续写作。在此我对她致以衷心的感谢。

Erklärung:

Ich versichere, dass ich diese Arbeit selbstständig verfasst und keine anderen als die angegebenen Quellen und Hilfsmittel benutzt habe.

Heidelberg, den _____ _____

Unterschrift